Versatile Antibacterial and Antioxidant Bacterial Cellulose@Nanoceria Biotextile: Application in Reusable Antimicrobial Face Masks

Jie Tang‡, Yuping Zhang‡, Xingfei Liu‡, Yichao Lin, Lihua Liang, Xiaofang Li, Gregori Casals, Xiangyu Zhou*, Eudald Casals*, Muling Zeng**

X. Liu, Y. Lin, J. Tang, L. Liang, Y. Zhang, X. Li, Dr. E. Casals, Dr. M. Zeng
School of Biotechnology and Health Sciences, Wuyi University, 99 Yingbing Middle Rd., Jiangmen, 529020, China
E-mail: eudaldcm@gmail.com, mulingzeng@163.com

Dr. G. Casals
Service of Biochemistry and Molecular Genetics, Hospital Clinic Universitari and The August Pi i Sunyer Biomedical Research Institute (IDIBAPS), Carrer de Villarroel, 170, 08036 Barcelona, Spain
Liver and Digestive Diseases Networking Biomedical Research Centre (CIBEREHD), Av. Monforte de Lemos, 3-5, 28029 Madrid, Spain.
Department of Fundamental Care and Medical-Surgical Nursing, Faculty of Medicine and Health Sciences, University of Barcelona, Barcelona 08007, Spain
E-mail: casals@clinic.cat

Dr. X. Zhou
Obstetrics and Gynecology Hospital of Fudan University, Shanghai Medical College, State Key Lab of Genetic Engineering, Fudan University, Shanghai 200011, China
Xiangyu Zhou: zhou_xiangyu@fudan.edu.cn

‡ J. Tang, Y. Zhang and X. Liu contributed equally to this work

Keywords: Functional Biotextiles; Bacterial Cellulose; Cerium Oxide Nanoparticles; Antioxidants; Antimicrobial Face Masks

Abstract. Despite considerable interest in medical and pharmaceutical fields, there remains a notable absence of functional textiles that concurrently exhibit antibacterial and antioxidant properties. Herein, we introduce a new composite fabric constructed using nanostructured bacterial cellulose covalently-linked with cerium oxide nanoparticles (BC@CeO_2NPs). The synthesis of CeO_2NPs on the BC is performed via a microwave-assisted, in-situ chemical deposition technique, resulting in the formation of mixed valence Ce^{3+}/Ce^{4+} CeO_2NPs. This approach ensures the durability of the composite fabric subjected to multiple washing cycles. The ROS-scavenging activity of CeO_2NPs and their rapid and efficient eradication of >99% model microbes, such as *Escherichia coli*, *Pseudomonas aeruginosa* and *Staphylococcus aureus* remain unaltered in the composite. To demonstrate the feasibility to incorporate the fabric in marketable products, we have fabricated antimicrobial face masks with filter layers made of BC@CeO_2NPs cross-linked with propylene or cotton fibers. These masks exhibit complete inhibition of bacterial growth in the three bacterial strains, improved breathability compared to respirator masks and enhanced filtration efficiency compared to single-use surgical face masks. This study provides valuable insights into the development of functional BC@CeO_2NPs biotextiles which design can be extended to the fabrication of medical dressings and cosmetic products with combined antibiotic, antioxidant and anti-inflammatory activities.

1. Introduction

Bacterial Cellulose (BC) has garnered significant attention for the development of various medical and cosmetic dressings owing to its outstanding mechanical and physical properties emerging from its unique three-dimensional highly-organized nanometric fiber mesh structure.[1] BC can be synthesized by various types of bacteria,[2] and the resulting product maintains the identical molecular formula as plant cellulose but does not contain lignin, hemicellulose, or pectin. This absence enables its production with high purity through relatively straightforward procedures.[3] BC also displays high tensile strength and thermal stability. The presence of hydrophilic OH^- groups within its structure facilitates the integration of various bioactive substances, leading to the creation of functional textiles. In this study, we have chosen to incorporate CeO_2NPs into the BC structure to develop a BC@CeO_2NPs composite fabric with antioxidant and antibiotic properties. None of the currently available dressings exhibit these combined activities,[4] which is subject of intense research efforts[4-5] for its potential e.g. in protection from bacterial-infection-induced wound healing/skin regeneration. In addition to exhibiting high biocompatibility, CeO_2NPs have consistently shown substantial biomedical effectiveness in the literature. They hay been highlighted as anti-inflammatory agents[6], and their broad-spectrum antibacterial[7] and antiviral[8] efficacy has been demonstrated. These remarkable properties are attributed to the CeO_2NPs' ability to participate in redox reactions through a well-described regenerative cycle between the Ce-oxidized (Ce^{4+}) and Ce-reduced (Ce^{3+}) states, resulting in the formation/loss of oxygen vacancies.[9]

To date, only a few studies have investigated the integration of CeO_2NPs into BC. These studies have predominantly utilized organic solvents like ethylene glycol and benzyl alcohol in the synthesis process. Alternatively, some studies have employed physical impregnation methods to introduce pre-synthesized CeO_2NPs.[10] Among those, none of them explored antibacterial or cellular ROS-scavenging effects. Petrova et al.,[10b] assessed the biocompatibility, Gofman et al.,[10a] their use in the process of stem cell proliferation, Melnikova et al.,[10e] the reduction and oxidation activities against selected molecules, and Van Gent et al.,[10d] the antioxidant potential against 2,2-diphenyl-1-picrylhydrazyl (DPPH assay). In addition, the optimal conditions for the preparation of BC@CeO_2NPs composites have not been thoroughly investigated, except for the recent work by Rocha et al., which focused on the influence of temperature.[10c] Thus, in a first part of this study, we have investigated the optimal reaction conditions for synthesizing BC@CeO_2NPs in aqueous solution. The impregnation of CeO_2NPs through in-situ chemical incorporation and oxidation

of the Ce^{3+} precursor, leading to covalently attached CeO_2NPs on the BC, is controlled by modifying the reaction parameters. The quantity and morphology of the CeO_2NPs remain unchanged following repeated washing steps. Subsequently, the biocidal effectiveness against *Escherichia coli*, *Staphylococcus aureus,* and *Pseudomonas aeruginosa* has been assessed, revealing nearly 100% inhibition of bacterial growth in all instances. Additionally, the ROS (Reactive Oxygen Species)-scavenging properties of the as-synthesized CeO_2NPs are maintained in the composites.

In a second part of this study we have employed the developed BC@CeO_2NPs films to craft innovative filtration layers and antimicrobial face masks. This serves as a demonstration of their practicality and potential for incorporation into marketable items. As known, the use of face masks, including surgical and respirator masks, is not entirely effective in completely blocking the transmission of virus or bacteria droplets and aerosols, even when properly sealed. This situation partly arises from the existence of airborne droplets that are smaller than the mesh size[11]. However, the primary issue lies in the impossibility to avoid inhaling respiratory particles emitted by another person due to their high concentration, surpassing the current capacity of face masks.[12] Moreover, the ubiquitous existence of bacteria in our environment and the well-documented fact that face masks, both inside and out, can easily harbor a variety of organisms, including pathogenic bacteria[13] underscores the need to develop efficient antimicrobial face masks. Research into textiles impregnated with nanomaterials to confer antimicrobial properties has increased in recent years.[14] These textiles typically incorporate copper, silver, zinc oxide (ZnO), or titanium oxide (TiO_2)[15] to damage viral or bacterial structures by releasing toxic Ag^+ and Cu^{2+} ions or generating oxygen radicals,[16] raising concerns regarding the leaching of toxic metals ions.[17] Moreover, the limited durability and non-reusability of most masks, along with their non-recyclability, contribute to increased waste generation and environmental concerns.

Herein, we have fabricated two types of antimicrobial face masks integrating an innovative filter layer composed of highly-stable BC@CeO_2NPs crosslinked with polypropylene (PP) or cotton fibers. CeO_2NPs offer a superior biocompatibility in contrast to other materials commonly employed to fabricate functional textiles such as silver, copper, or transition NPs.[6a] Additionally, the BC@CeO_2NPs possesses high porosity, a large surface area, and outstanding air and water permeability, thus displaying improved filtration efficiency and breathability in comparison to non-woven fabrics. BC is also a recyclable material that can help mitigate the environmental impact of current face masks. The comprehensive assessment of filtration efficacy and differential pressure drop (indicating

respiratory comfort) for the fabricated face masks containing BC@CeO_2NPs has revealed outstanding quality factor (QF) results. Consequently, our innovative approach provides a straightforward and cost-effective technique for manufacturing antimicrobial face masks, which can also be extended for the fabrication of other medical and cosmetic products exhibiting dual anti-inflammatory and antibacterial properties, as demonstrated in this study.

2. Results

2.1. Optimization of the reaction conditions of BC@CeO_2NPs synthesis

BC was synthesized under static culture conditions, resulting in the formation of a cellulose membrane at the interface between the liquid and air, following a procedure similar to our previous work.[2, 18] For the preparation of BC@CeO_2NPs, in-situ synthesis of CeO_2NPs within the wet BC matrix was chosen as the method of incorporation. The choice of in situ chemical deposition over alternative techniques like mechanical blending and physical incorporation (such as impregnation or electrostatic assembly of pre-synthesized NPs was motivated by its capability to attain heightened stability and a more uniform dispersion of NPs within the BC matrix. Although physical loading methods offer easier functionalization conditions, materials incorporated through these methods tend to shed due to weak interactions.[19] Furthermore, the use of wet BC enables the incorporation of a larger amount of metallic precursor due to the higher number of accessible OH^- groups and the subsequent increase in NP formation.[18] **Figure 1** depicts the steps involved in the preparation of BC@CeO_2NPs. In a typical synthesis, BC membranes harvested after three days of culture using *Komagataeibacter Xylinus* (*K. Xylinus*) were immersed in microwave-oven flasks containing an aqueous solution of cerium nitrate hexahydrate as the cerium (Ce^{3+}) precursor (10 mM, final concentration). The microwave-assisted reaction was conducted subsequent to the introduction of aqueous ammonia (NH_4OH) as the oxidizing agent (27 mM, final concentration). **Figure S1** and **Video S1** shows the images of the resulting BC@CeO_2NPs membranes, which were dried through solvent evaporation at room temperature (BC-RD) or through freeze-drying by sublimation of the frozen solvent (BC-FD).

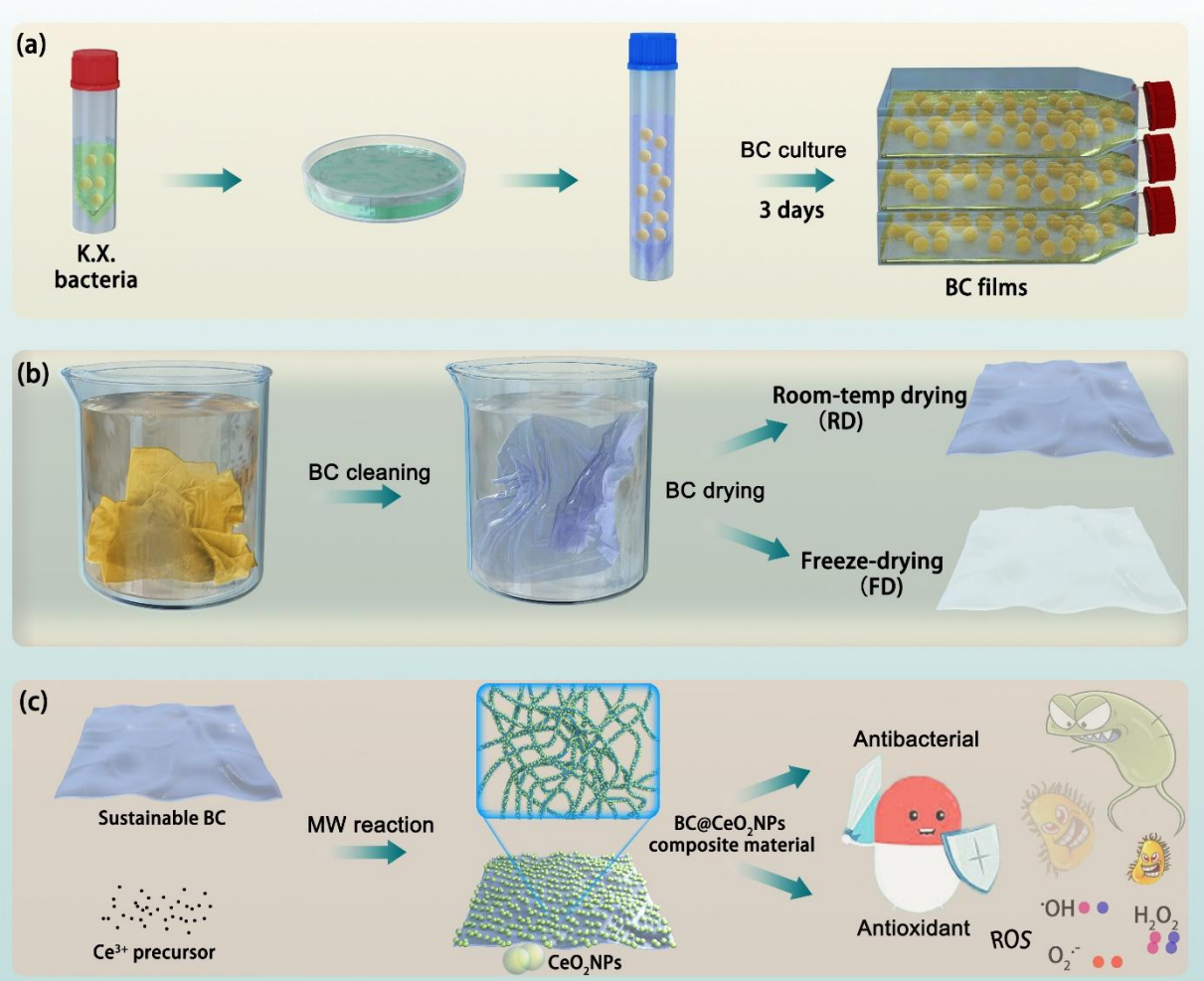

Figure 1. Schematic illustration of the formation of the BC@CeO_2NPs membranes with combined antibacterial and antioxidant activities. **A.** The synthesis begins with the harvesting of *K. Xylinum* culture for 3 days to obtain the BC membrane. **B.** After cleaning, the membranes are dried via two different methods, namely solvent evaporation at room-temperature (RD) or freeze-drying by sublimation of the frozen solvent (FD). **C.** The microwave-assisted in-situ chemical synthesis of crystalline CeO_2NPs covalently linked to the BC structure takes place via incorporation of the Ce^{3+} precursor in the wet (undried) BC membrane and further pH increase. These results in a stable BC@CeO_2NPs membranes that are dried as in B.

The synthesis of CeO_2NPs through the oxidation of a cerium salt (mainly nitrate or chloride) under basic conditions is well-documented in the literature and it is known to yield monodisperse small-sized CeO_2NPs.[20] To determine the optimal conditions for the preparation of BC@CeO_2NPs composites, the factors that may influence the microwave-assisted synthesis of CeO_2NPs were first thoroughly investigated. Our aim was to establish optimal conditions that would ensure the formation of monodisperse and stable CeO_2NPs without altering the structure of the BC membranes. We investigated the impacts of different heating rates and reaction times, spanning from 0.1 °C/s to 2.5 °C/s and 1 to 10 minutes across a range of temperatures (60–180 °C), MW power levels (350–850 W), and stirring speed (200–600 rpm). A total of 64 samples were generated, and their physicochemical

characteristics were analyzed using a combination of Transmission Electron Microscopy (TEM), UV-VIS spectroscopy, and Dynamic Light Scattering (DLS) **(Figures S2-S3, Table S1).** Our findings indicate that temperature and reaction time are crucial for the optimal synthesis of CeO_2NPs. Specifically, a reaction time of 3 min at 150 °C was identified as the condition that facilitated a complete reaction of the precursor, resulting in the formation of the CeO_2NPs within the shortest time frame **(Figure S2a, c)**. Significantly, in examining the impact of temperature, it was observed that temperatures lower than 150 °C did not lead to the complete conversion of the Ce precursor into CeO_2NPs, evidenced by the presence of a peak around c.a. 260 nm in the UV-VIS spectra, indicating Ce^{3+} absorbance.[21] Conversely, the highest temperature of 180°C exhibited UV-VIS spectra very similar to those of the synthesis conducted at 150°C, suggesting that raising the temperature beyond this point had negligible influence on the resultant CeO_2NPs. Conversely, an increased stirring speed had a detrimental effect on the stability of the CeO_2NPs, likely due to excessive energy introduction that led to particle coalescence (**Figure S2b)**.[22] On the other hand, MW power (from 350 W onwards) had minimal to no effect on the synthesis process. Hence, the optimized parameters for attaining the briefest reaction period and lowering energy usage in the BC@CeO_2NPs synthesis were identified as follows: a reaction time of 3 minutes at 150 °C, attained through a heating rate of 2 °C/s for 1 min, MW set at 350 W, and an agitation speed of 200 rpm. Additionally, we investigated the influence of pH (ranging from 8 to 13) by varying the amounts of precursor and NH_4OH. Our results (optimal Ce^{3+}:NH_4OH ratio of 1:2.7; pH~11) align with previously reported findings.[10c, 20, 23]

2.2. Morphology, structural, and physicochemical properties of the BC@CeO_2NPs.

Figure 2a illustrates the CeO_2NPs synthesized under optimized conditions in BC-RT membranes, with a mean diameter of 5.45±0.44 as calculated from TEM image analysis **(Figure S3)**. Unless explicitly specified, all subsequent results presented are based on these membranes. **Figure 2b** and **c** display TEM and SEM images of the pristine BC revealing its characteristic 3D porous network structure, which has been extensively characterized in previous studies.[2, 18] The morphological features of BC@CeO_2NPs are depicted in **Figure 2d-g**. SEM images of BC@CeO_2NPs display similar BC fibrils as seen on the surface of the pure BC film, but with an abundance of CeO_2NPs **(Figure 2d)**. The CeO_2NPs appear as brighter spots, forming a denser network structure within the membranes. This confirms that the nanometer-sized BC fibers, interconnecting to form a finely woven porous structure, facilitate the even diffusion of Ce^{3+} ions throughout the BC matrix. Moreover, line scan

analysis of Ce obtained from SEM images across a large area reveals no significant gradients, indicating the homogeneous distribution of CeO_2NPs on the BC **(Figure 2e)**. TEM images **(Figure 2f-g**) show that CeO_2NPs are located on the BC fibrils, covering them entirely, with no CeO_2NPs observed within the pores. This affirms the initiation of CeO_2NPs on the hydroxyl moieties of bacterial cellulose, aligning with a comparable mechanism documented for different inorganic NPs.[18, 24] The process is akin to the one detailed by Karakoti et al. for creating CeO_2NPs on diverse hydroxylated polymer interfaces.[25] This process involves the anchoring and stabilization of Ce^{3+} ions by the high density of hydroxyl groups on the BC fibrils, which undergo hydrolysis and oxidation to form CeO_2NPs due to the pH increase resulting from the addition of ammonia. Analysis of the HR-TEM image reveals the presence of (111) planes of face-centered cubic (FCC) CeO_2 **(Figure 2g**, inset), and the indexed electron diffraction pattern recorded in selected area mode (SAED in **Figure 2g,** inset) demonstrates the FCC lattice structure corresponding to crystalline CeO_2NPs within the nanocomposites.

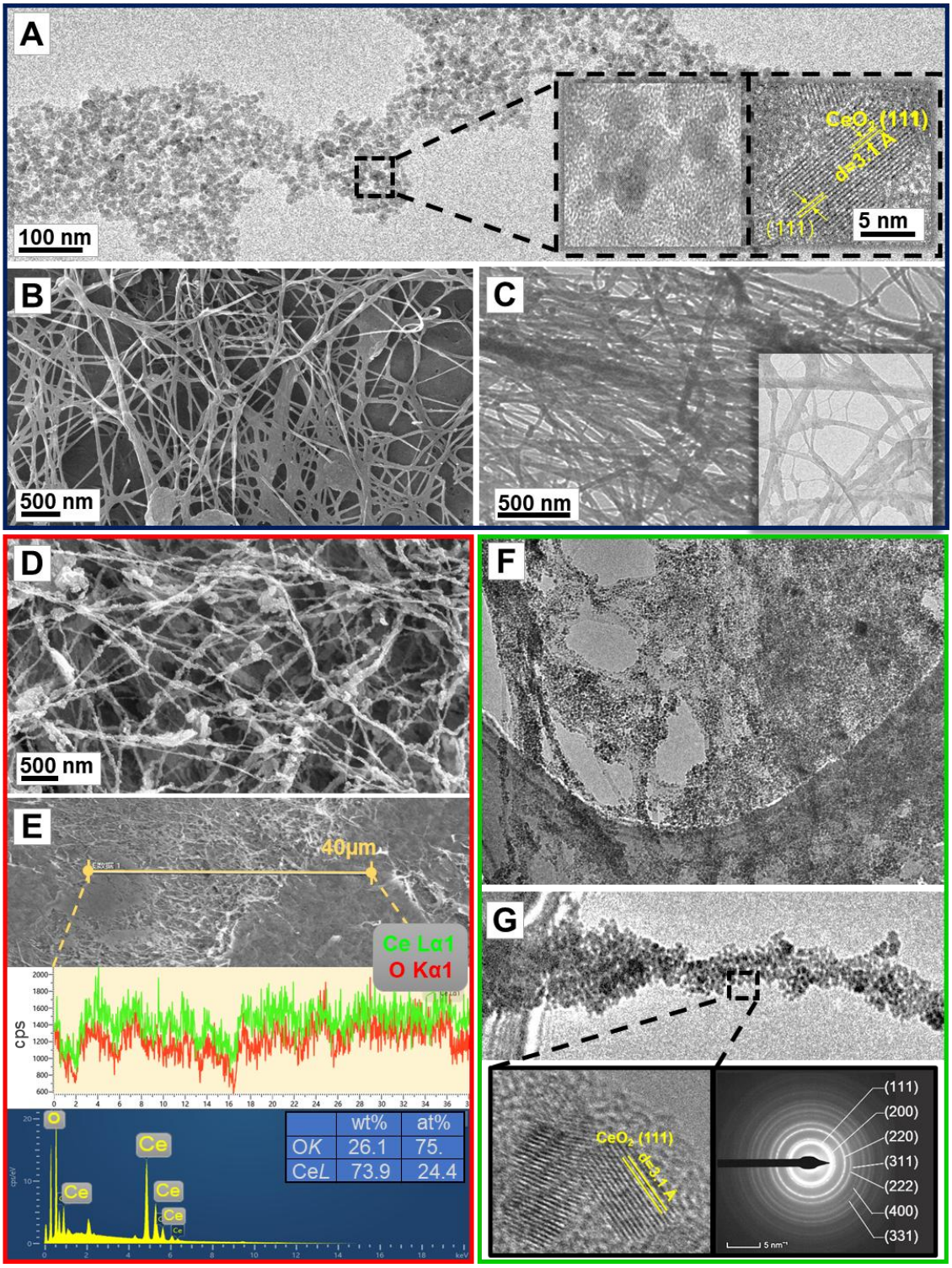

Figure 2. Morphology and surface properties of the BC@CeO_2NPs. **A.** TEM images of the CeO_2NPs synthesized under optimized conditions, displaying the (111) planes of the face-centered cubic CeO_2 phase (inset). **B-C.** SEM and TEM images, respectively, of the pristine BC. **D.** SEM image at the same magnification as B, showing BC@CeO_2NPs, where CeO_2NPs can be observed as brighter spots crowding the surface of the BC membranes. **E.** SEM image of a larger area of BC@CeO_2NPs and line scan analysis, demonstrating the ubiquitous presence of Ce. **F-G.** TEM images at different magnifications, revealing CeO_2NPs covering the entire BC structure with no CeO_2NPs observed within the pores. Insets correspond to the analysis of the HR-TEM image, showing the (111) planes of the face-centered cubic CeO_2 phase, as well as the **i**ndexed electron

diffraction pattern recorded in selected area mode (SAED), demonstrating the FCC lattice structure. For clarity, the blue frame represents the characterization of CeO_2NPs and BC controls, while the red and green squares indicate SEM and TEM analysis of BC@CeO_2NPs, respectively.

To gain a deeper understanding of the integration of CeO_2NPs on the BC surface, elemental mapping for Ce and O was performed on a large area of the BC@CeO_2NPs sample. **Fig. 3a** displays the elemental mapping of Ce obtained from STEM images, confirming the highly uniform distribution of CeO_2NPs within the BC structure. The semi-quantitative determination of the Ce/O ratios through EDS analysis is also consistent across both large and small areas of analysis **(Figure 2e and 3b)**. The presence of CeO_2 is further supported by the appearance of characteristic emission lines of Ce at 4.55 keV (Ce Lα) and 5.26 keV (Ce Lβ) in the EDS spectra **(Figure 3b)**. Furthermore, the physicochemical properties of BC@CeO_2NPs were investigated through a combination of XRD, XPS, FT-IR, and BET analyses **(Figure 3c-f, Figure S4)**. The XRD patterns of the as-synthesized CeO_2NPs and the BC@CeO_2NPs **(Figure 3c)** demonstrate the maintenance of CeO_2 particle size and crystallinity. The diffraction peaks corresponding to the (111), (200), (220), and (311) planes of the fluorite (cubic) CeO_2 phase (JCPDS No 34–0394), observed at 28.6°, 33.1°, 47.5°, and 56.3°, respectively, are evident in the BC@CeO2NPs. However, their intensity is reduced due to the interactions between CeO_2 and the BC matrix, and other less intense peaks at higher 2θ degrees are barely or not visible. This diminished visibility is likely due to the relatively modest quantity of CeO_2NPs present within the composite compared to the mass of BC.. Furthermore, the crystalline sizes of the as-synthesized CeO_2NPs (6.91 nm) and those in the BC (6.59 nm), calculated using Scherrer's formula from the XRD data by considering the Full Width at Medium Height of the CeO_2 (111) reflection, align with the values obtained from TEM analysis **(Figure S3)**. The slightly reduced mean crystallite size of CeO_2NPs in the BC, as observed from the width of the 28.6° peak (**Figure 3c**, inset), suggests that the BC may have served as a template for increased CeO_2 nucleation.[18] In addition, the two prominent reflections that are characteristic of the ordered structure of the I polymorphs of bacterial cellulose, with intensity peaks at 2θ regions of 14.5° and 22.7° are also observed. These correspond to the diffraction planes of (101) and (002) of crystalline cellulose (JCPDS No 03–0829).

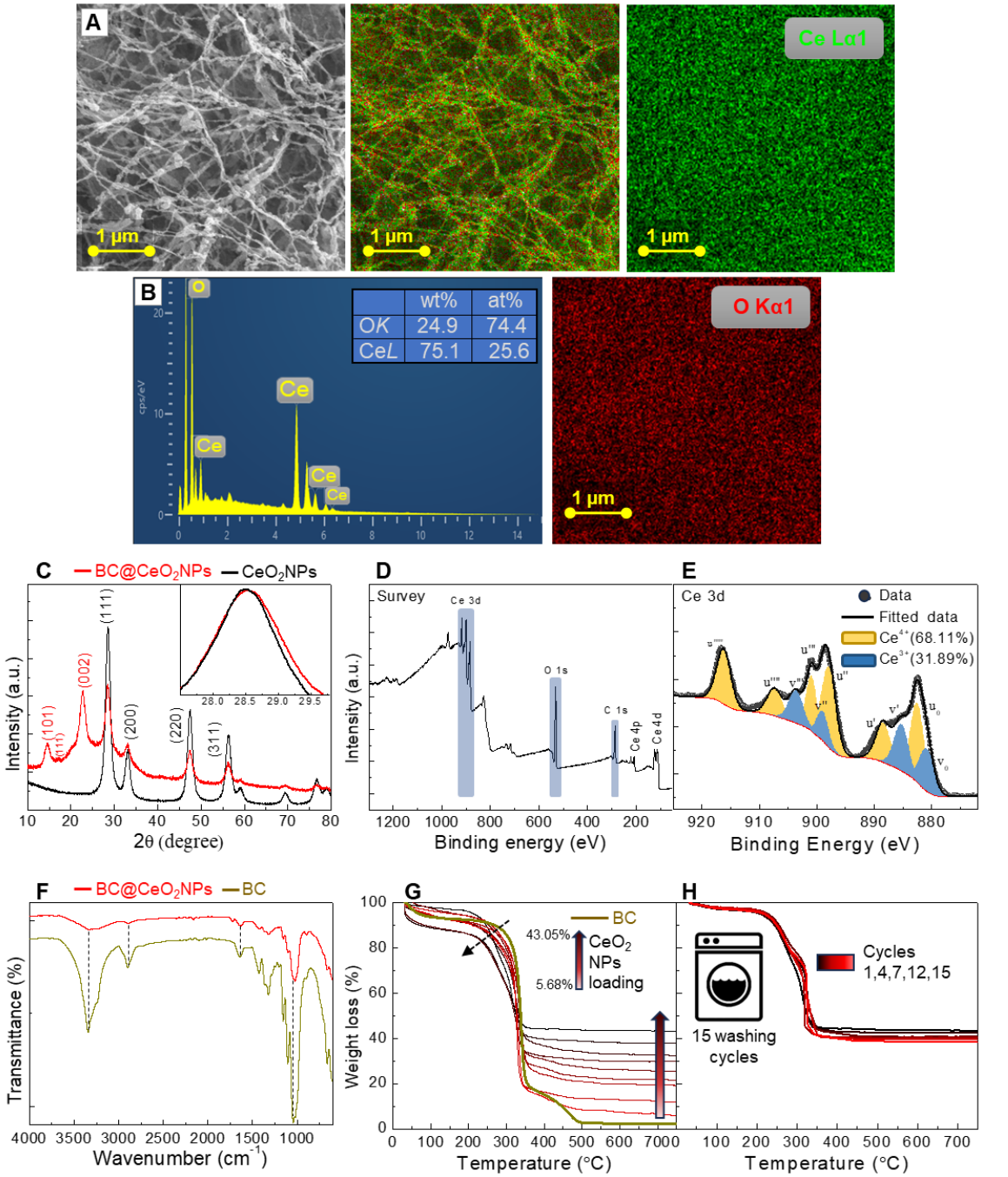

Figure 3. Structural properties, CeO_2NPs impregnation control and stability of the BC@CeO_2NPs. **A.** SEM image of BC@CeO_2NPs with corresponding overlapping elemental maps of Ce and O. **B.** EDS spectrum. **C.** XRD patterns of CeO_2NPs and BC@CeO_2NPs. **D.** XPS survey scan and **E.** Ce 3d core-level spectra of CeO_2NPs in the BC. **F.** FT-IR spectra of BC and BC@CeO_2NPs. **G.** TGA of BC membranes and BC@CeO_2NPs synthesized with increasing amounts of Ce precursor (from 0.1 to 10 mM) resulting in higher percentages of stable inorganic residues (from 5.68% to 43.05%) . **H.** TGA of BC@CeO_2NPs after undergoing 15 washing cycles. In G and H the gradient of red color gradually progressing from lighter tones to darker hues indicates the progression from lower to higher values.

Additionaly, the FTIR spectra of pristine BC and BC@CeO_2NPs **(Figure 3f)** reveal comparable distinct peaks. This suggests that the development of CeO_2NPs did not bring about any modifications to the inherent structure of the BC membranes. The prominent peak at 3200–3600 cm^{-1} is associated to the O–H stretching vibration, and other peaks correspond to the C–H stretching vibration (2800–3000 cm^{-1}), carbonyl (C=O) stretching vibration (1640 cm^{-1}), and C–O stretching vibration (1050–1150 cm^{-1}). These stretching vibrations are slightly weaker in the case of BC@CeO_2NPs due to the presence of NPs on the BC surface. Furthermore, BET measurements confirm the presence of CeO_2NPs within the BC matrix, as evidenced by a decrease in the mean pore width of BC@CeO_2NPs (5 nm) compared to pristine BC (29 nm), leading to an increased surface area **(Figure S4)**.

To investigate the chemical state and oxidation state of the CeO_2NPs on the BC surface, the Ce 3d core level region of the XPS spectra was analyzed **(Figure 3e)**. The Ce 3d peak is complex due to its associated peak structure. It consists of two groups of peaks corresponding to the 3d5/2 and 3d3/2 spin orbitals, along with a satellite peak at 916.51 eV that serves as a fingerprint of Ce^{4+} compounds.[8a, 26] One group of peaks at 882 eV corresponds to the 3d5/2 orbital, while another group at 901 eV corresponds to the 3d3/2 orbital. The asymmetric nature of these peaks is attributed to a mixture of Ce^{3+} and Ce^{4+} states in the CeO_2NPs structure,[8a, 27] with the peaks labeled as v_0, v', v'', v''' (in blue) associated with Ce^{3+} and the peaks labeled as u_0, u', u'', u''', u'''', u''''' (in yellow) associated with Ce^{4+} oxidation states. Based on non-linear least squares fitting, the relative content of Ce^{3+} and Ce^{4+} is determined to be 31.89% and 68.11%, respectively, resulting in a Ce^{3+}/Ce^{4+} ratio of 0.47. Additionally, the survey plot **(Figure 3d)** displays the presence of the three main elements (O, Ce, and C), with the dominant peak observed at 530 eV (O 1s core level), indicating the lattice of metal oxides such as CeO_2.

2.3. Stability and impregnation control of CeO_2NPs in the BC@CeO_2NPs

TGA, a widely utilized method for determining the thermal properties of BC, was also employed to investigate the incorporation of CeO_2NPs in BC and their stability during washing cycles **(Figure 3 g-h)**. In the initial experiments, nine BC@CeO_2NPs membranes were prepared with increasing concentrations of the Ce precursor from 0.1 to 10 mM while maintaining a $Ce(NO_3)_3$:NH_4OH ratio of 1:3. The TGA curves of these samples were compared with that of pristine BC. The weight loss curve of the pristine BC control sample in the air follows the characteristic pattern observed in BC films. It exhibits three distinct regions. Firstly, a slight weight loss at around 30–180 °C, which is associated with water

vaporization and the decomposition of proteins and volatile impurities[28] (approximately 4% in our BC films). Secondly, a sharp decrease in weight loss between 180–360 °C indicates the main stage of BC pyrolysis, resulting from cellulose decomposition, including simultaneous dehydration, depolymerization, and decomposition of polysaccharide monomeric units. Finally, from 360–500 °C, complete BC pyrolysis occurs, where the monomeric products formed in the second stage degrade in an oxygen-containing atmosphere, leaving behind residual non-volatile products,[10a] which account for 2.01% of our pristine BC sample.

A similar trend, with some variations, is observed in the TGA curves of the BC@CeO_2NPs samples after the organic component has completely volatilized **(Figure 3g)**. In these cases, the increased concentration of the initial Ce precursor leads to higher percentages of stable inorganic residues, ranging from 5.68% to as high as 43.05%. Taking the 2.01% as residues coming from BC (indicated by the yellow line in **Figure 3g**), the mass fraction of CeO_2NPs in the different samples is calculated to range from 3.67% to 41.04%, with increasing Ce^{3+} precursor concentration (from 0.1 to 10 mM). TEM images support this observation, showing that the amount of CeO_2NPs in the BC fibers progressively increases with higher precursor amounts **(Figure S5)**. These findings illustrate that our microwave-assisted synthesis methodology permits the fabrication of BC@CeO_2NPs composites featuring a controllable quantity of CeO_2NPs. Additionally, it is noteworthy that the intense decomposition process (first stage of pyrolysis) shifted to lower temperatures as the amount of CeO_2NPs in the BC increased. This can be attributed to the catalytic activity of CeO_2NPs in the decomposition of various organic compounds,[29] indicating that this activity is maintained in the BC@CeO_2NPs. Importantly, after the post-synthesis washing process, which removes non-attached CeO_2NPs from the BC@CeO_2NPs composites, subsequent washes had minimal impact on the amount of NPs even after 15 laundry cycles. The TGA plots **(Figure 3h)** show less than 5% leaching of Ce ions or CeO_2NPs, indicating that the microwave-assisted in-situ chemical synthesis ensures excellent stability of the CeO_2NPs on the surface of the BC membranes.

2.4. Antibacterial and ROS-Scavenging activity of BC@CeO_2NPs

Bioactive multifunctional antibacterial and antioxidant properties of the synthesized BC@CeO_2NPs are shown in **Figure 4 and Figure S6-7**. First, a quantitative assessment of the impact of BC@CeO_2NPs on bacterial growth kinetics was conducted by incubating them with three distinct strains: *Escherichia coli* and *Pseudomonas aeruginosa* (*E. coli* and *P. aeruginosa*, both gram-negative bacteria), and *Staphylococcus aureus* (*S. aureus*, gram-

positive bacteria). This was followed by optical density spectrophotometric measurements at 600 nm (OD_{600}) of the culture medium **(Figure 4a)**. After incubation with circular cutouts (d=1.5 cm) of BC@CeO_2NPs membranes containing c.a. 20% CeO_2 (w/w) as determined by TGA analysis, bacteria were almost undetectable. The antibacterial rate of the BC@CeO_2NPs to *E. coli*, *P. Aeruginosa* and *S. aureus* was over 99% in all cases **(Figure 4b)**. Analysis of the curves revealed lack of exponential (log) phase in any of the strains, signifying almost complete inhibition of bacterial cell growth, thus showing the significant broad-spectrum antibacterial activity of the composite **(Figure 4c)**. Control experiments involving bacteria exposed to CeO_2NPs, synthesized using the microwave-assisted technique, were executed at a concentration of 1 mg/mL. This specific concentration has been acknowledged in previous research for its antibacterial attributes[7c, 7e, 30] and is even lower than the computed amount present in the BC@CeO_2NPs **(**as indicated in **Figure S6)**. In the case of CeO_2 nanoparticles, a growth inhibition c.a. 85-95% was attained upon incubation with the three bacterial strains **(Figure 4c)**. Another set of experiments involving bacteria exposed to pristine BC showed no inhibition of bacterial growth **(Figure S8)**.

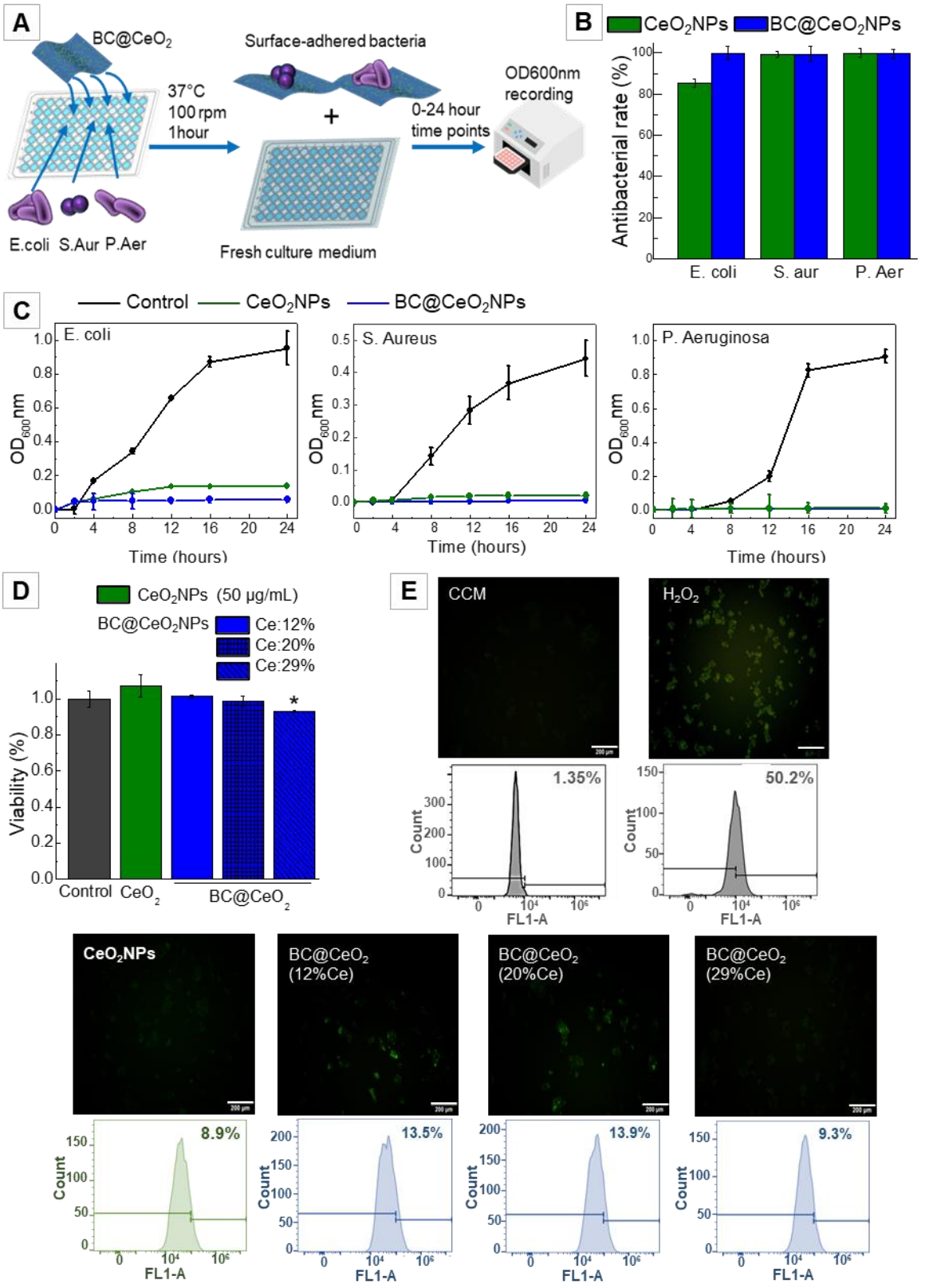

Figure 4. A. Schematic illustration of the antibacterial experiments with BC@CeO_2NPs membranes. Growth inhibition of *E. coli*, *S. aureus*, and *P. aeruginosa* by CeO_2NPs and BC@CeO_2NPs (content of CeO_2 c.a. 20% (w/w)) was measured by optical density at 600 nm (OD_{600}) at various time points and the inhibition rate was calculated respect to controls. **B.** Antibacterial rates calculated at the 16-hour mark for the CeO_2NPs and BC@CeO_2NPs. **C.** The OD_{600} measurements at different time points. **D.** Cell viability in A549 cells incubated

with CeO_2NPs (50 µg/mL) synthesized through the microwave-assisted method and BC@CeO_2NPs containing c.a.12%, 20% and 29% of CeO_2. Values are the mean of three independent experiments, with error bars representing the standard deviation; *$p < 0.05$ compared with control. **E.** Flow cytometric analysis of reactive oxygen species (ROS) generation using DCFH-DA fluoroprobe in A549 and corresponding representative images of the immunofluorescence staining of A549 cells. Decreased diffused green fluorescence is visible in all cases compared with cells treated with H_2O_2. Scale bar 200 µm.

The biocompatibility and ROS-scavenging properties in A549 cell line of CeO_2NPs synthesized through the microwave-assisted method and BC@CeO_2NPs were assessed with MTS and DCFH-DA assays, respectively. For these experiments, CeO_2NPs were employed at a concentration of 50 µg of CeO_2/mL, since higher concentrations displayed toxic effects **(Figure S7)**, which is in line with the literature.[6a, 31] Different BC@CeO_2NPs containing 12%, 20% and 29% of CeO_2 were also used. **Figure 4d** illustrates that both the CeO_2NPs and the BC@CeO_2NPs loaded with 12% and 20% CeO_2 demonstrated similar cell viability compared to the control group, indicating their excellent biocompatibility. However, in the case of the sample loaded with 29% CeO_2NPs, although cell viability remains around 90% compared to the control, it is statistically lower. Therefore, the loading amount of 20% CeO_2 was chosen for the antibacterial experiments and the development of face mask prototypes based on BC@CeO_2NPs membranes. Regarding the analysis of the ROS-scavenging properties **(Figure 4e)**, flow cytometric analysis of ROS generation using DCFH-DA fluoroprobe showed that H_2O_2 treated cells experienced a 50.2% increase in ROS generation with respect to untreated cells. Cells were further incubated 24 hours with CeO_2NPs and the different BC@CeO_2NPs. In this instances, increased ROS generation was only 8.9% in the case of CeO_2NPs and, 13.5%, 13.9% and 9.3% in the case of BC@CeO_2NPs containing 12%, 20% and 29% of CeO_2 respectively. This represents a 82.3% decrease with respect to H_2O_2-treated cells in the case of CeO_2NPs, and 73.1%, 73.3% and 81.5% in the case of the differently loaded BC@CeO_2NPs, indicating that CeO_2NPs effectively protect cells from oxidative damage and that this property is maintained in the composites.

These results attributed to the BC@CeO_2NPs membrane promising potential for applications such as the fabrication of medical dressings with dual antioxidant and antibacterial properties. The antibacterial[7] and antiviral[8] attributes of CeO_2NPs have been substantiated in various studies. Noteworthy, the precise antibacterial mechanism of CeO_2NPs remains a topic of contention, and a uniform agreement is elusive across the range of investigations. For example, different studies have highlighted that the antibacterial efficacy

of CeO_2NPs is intensified when the NPs carry a positive charge.[7d, 32] This may be due to the advantageous electrostatic attraction towards the negatively charged cell membranes of both gram-negative and gram-positive bacteria. However, the CeO_2NPs produced using our method exhibit negatively charged surfaces, reflected by a Z-potential of -31 mV at a pH of 7. Other investigations propose that in the presence of oxygen, Ce^{4+} has the capacity to catalyze the generation of reactive oxygen species (ROS), such as superoxide radicals ($O_2^{\cdot-}$), hydrogen peroxide (H_2O_2), and hydroxyl radicals (·OH). These ROS subsequently act upon cellular elements such as lipids, proteins, and DNA, leading to the disruption of critical cellular functions.[7c] However, few studies have attempted to elucidate how CeO_2NPs exhibit such pro-oxidant traits in conjunction with the robust antioxidant and anti-inflammatory properties in human cells and model animals by mimicking the activity of several key endogenous enzymes, e.g. superoxide dismutase (SOD),[33] and catalase.[34] The distinct feature of rare earth elements, like Ce, is the presence of 4f orbitals shielded by 4d and 5p orbitals which implies that the 4f electrons are weakly bound to the nucleus and allows for the coexistence of both Ce^{3+} and Ce^{4+} ions on their surface.[9b] This enables the formation and occupation of oxygen vacancies, acting CeO_2 as electron donor or acceptor[35] and making CeO_2 an effective catalyst for both oxidation and reduction reactions. Thus, CeO_2 has been described as "redox-buffer",[9b] and along with the low reduction potential of CeO_2 allows the maintenance of the redox balance of cells or tissues by scavenging free radicals only when they are in excess [9b, 35], therefore enabling the widely reported beneficial anti-inflammatory and antioxidant activities for the prevention and treatment of many diseases associated with chronic inflammation.[6a] Accordingly, some researchers suggest that the mixed-valence and ROS buffering features of CeO_2NPs may disrupt the electron flow and respiration of bacteria upon adsorption onto the bacterial cell membrane where the respiration-related electron transport chain occurs.[36]

2.5. Fabrication of BC@CeO_2NPs-functionalized filter layers

To explore the effectiveness of applying the developed BC@CeO_2NPs in commercial products, we proceeded to develop various filter layers and prototypes of face masks and subsequently evaluated their antibacterial properties **(Figures 5-6 and Fig S6)**. Different techniques for functionalizing face masks have been described in previous studies, such as coating the mask with functional materials or incorporating a layer of functional material between the inner and outer layers.[37] In our approach, we initially prepared single layers of cotton or non-woven polypropylene (PP) that were crosslinked with BC@CeO_2NPs (referred

to as Cotton@BC@CeO_2NPs and PP@BC@CeO_2NPs). To fabricate these filter mask layers, BC was generated in situ on PP or cotton films by incubating them with *K. Xylinum* under the conditions described earlier. This resulted in strong van der Waals and hydrogen bonding interactions between BC and the PP or cotton fibers, forming stable composites as previously reported for BC crosslinked with PP, cotton, microcrystalline cellulose, and graphene oxide, among others.[38] The PP@BC and cotton@BC layers were further purified and placed in MW tubes, where $Ce(NO_3)_3 \cdot 6H_2O$ and NH_4OH were added for the microwave-assisted synthesis of BC@CeO_2NPs, following the procedures outlined in this study, resulting in the final PP/Cotton@BC@CeO_2NPs layers. The thickness of the bacterial cellulose (BC) membrane can be modulated by the duration of cultivation. In our instance, with a cultivation period of 5 days, the BC@CeO_2NPs membranes possessed a thickness of c.a. 100 µm. For comparison, the middle melt-blown filtration layer found in KN95 and analogous respirator masks typically ranges from 100 to 500 µm.[39]

Figure 5a-d display STEM photographs and corresponding elemental mapping of Ce and O, clearly showing the BC membranes incorporating CeO_2NPs covering micrometric fibers of either PP or cotton. The presence of CeO_2 is further supported by the appearance of characteristic emission lines of Ce at 4.55 keV (Ce Lα) and 5.26 keV (Ce Lβ) in the EDS spectra **(Figure 5b, d)**. Based on the TGA results **(Figure 5f)**, the amount of CeO_2NPs in the fabrics is similar to that in the BC@CeO_2 synthesis. Specifically, using the same concentration of reagents to obtain approximately 20% CeO_2, it was calculated to be 17.2% for the BC@CeO_2 composite, 15.5% for Cotton@BC@CeO_2NPs, and 14.0% for PP@BC@CeO_2NPs. This slight decrease can be attributed to the reduction in the number of OH- reactive sites of the BC when adhered to the PP or cotton.

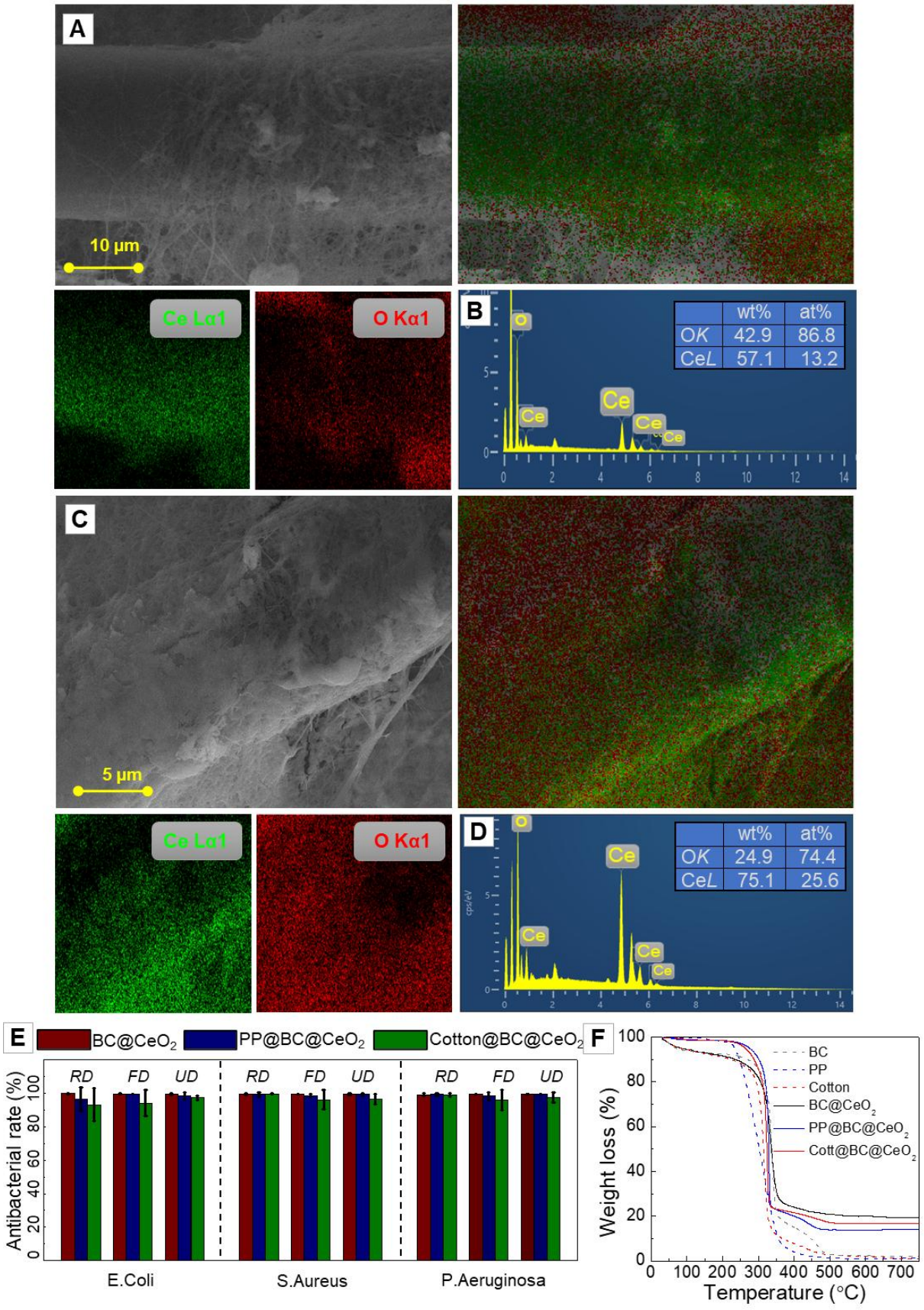

Figure 5. Characterization and antibacterial activity of PP@BC@CeO_2NPs and Cotton@BC@CeO_2NPs filter layers. **A.** SEM image of the PP@BC@CeO_2NPs with corresponding overlapping and elemental maps of Ce and O. **B.** EDS spectrum corresponding to the STEM image analysis shown in A. **C.** STEM image of

Cotton@BC@CeO_2NPs with corresponding overlapping and elemental maps of Ce and O. **D.** EDS spectrum corresponding to the SEM image analysis shown in C. **E.** Antibacterial rates calculated at 16 hour of incubation with *E. coli*, *S. aureus*, and *P. aeruginosa* measured by optical density at 600 nm (OD_{600}) for the various materials BC@CeO_2NPs undried (UD), dried at room temperature (RD), freeze-dried (FD) in red, the resulting PP@BC@CeO_2NPs in blue, and Cotton@BC@CeO_2NPs in green. **F.** TGA analysis of the BC@CeO_2NPs membrane and PP/Cotton@BC@CeO_2NPs layer showing similar CeO_2NPs content..

2.6. Antibacterial properties and Stability of filter layers prepared by different drying methods

Figure 5e shows the rate of *E. coli*, *P. Aeruginosa* and *S. Aureus* inhibition when the bacteria were incubated with different filter layers following the OD_{600}nm spectrophotometric measurements as described previously for BC@CeO_2NPs. For these experiments, we aimed to compare the antibacterial efficiency of the BC@CeO_2NPs dried by solvent evaporation at RT (BC(*RD*)@CeO_2NPs), as shown in **Figure 4b,** against the undried (wet) material (BC(*UD*), considering that moist conditions could promote bacterial growth of bacteria. Furthermore, a comparison was conducted between BC@CeO_2NPs subjected to freeze-drying (BC(*FD*)@CeO_2NPs) and the undried version, aiming to ascertain if the preparation procedure exerts an influence on the antibacterial attributes of BC@CeO_2NPs. Subsequently, several filter layers of PP/Cotton@BC@CeO_2NPs were also prepared using differently dried or undried BC@CeO_2NPs membranes and also tested and compared. In all instances, antibacterial rates of >95% were achieved **(Figure 5e)** showing the highly antibacterial efficiency of BC@CeO_2NPs is maintained in the filter layers. Further, the agar zone of the inhibition test was applied to the various BC@CeO_2NPs membranes and PP/Cotton@BC@CeO_2NPs at different levels of wetness (0–100%). This test provides a cost-effective, swift, and straightforward qualitative approach that manufacturers of antimicrobial surfaces utilize to compare their products' inhibition capacities. It enabled us to assess 60 samples of different membranes and layers with varying wetness degrees across the three bacterial strains. This was instrumental in investigating if film persistent wetness (potentially caused by factors such as respiration) could destabilize the BC@CeO_2NPs structure. The zone of inhibition area, although present, is expected to be significantly reduced if the antimicrobial agent is covalently attached to materials like textiles or polymers.[40] The zones of inhibition around the samples of BC@CeO_2NPs, PP@BC@CeO_2NPs, and Cotton@BC@CeO_2NPs with varying degrees of wetness are depicted in **Figure 6.** The average diameters of the inhibition zones of the different materials and membranes are recorded in **Tables S2-S5**. Similar to the optical density measurements, the average diameters for the BC@CeO_2NPs controls and filter

layers are comparable, with values around 5–7 mm. These results affirm that, while some inhibition occurs around the samples, negligible or no CeO_2NPs leak from the BC structure into the agar medium. This also substantiates the high stability of the CeO_2NPs within the BC structure, regardless of the wetness degree, confirming TGA results.

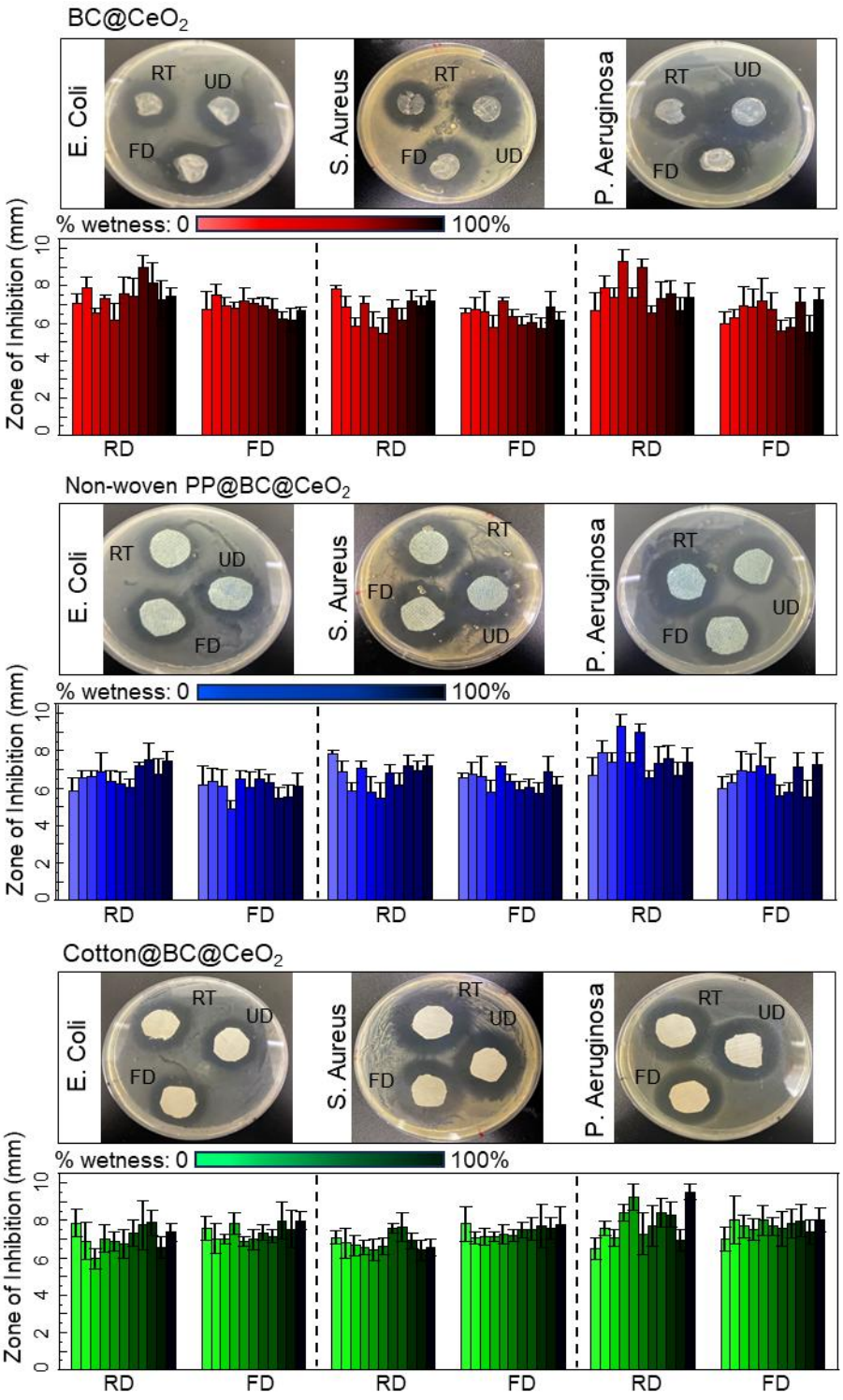

Figure 6. The inhibition zone of BC@CeO_2NPs (in red), PP@BC@CeO_2NPs (in blue), and Cotton@BC@CeO_2NPs (in yellow) against *E. coli*, *S. aureus*, and *P. aeruginosa* (n=3). BC@CeO_2NPs membranes and filter layers were tested as undried material or dried either at room temperature (RD) or freeze-dried (FD). For this two latter, the tests were performed with varying degrees of wetness (0–100%) and images correspond to 100% degree. It can be observed that low antibacterial effect is shown in all cases due to the strong attachment of the CeO_2NPs to the fabrics even at high-wetted conditions.

2.7. Face masks incorporating PP@BC@CeO_2NPs and PP@BC@CeO_2NPs filter layers: Filtration Efficiency, Inhalation Resistance, and Resulting Filter Quality Factors

Face mask prototypes were created by adding a second layer of non-woven, skin-friendly PP. **Figure 7a** depicts a schematic of the final face mask prototypes, and **Figure 7b, d, e,** and **g** display images of the masks along with SEM photographs of Cotton@BC@CeO_2NPs and PP@BC@CeO_2NPs filter layers at different magnifications. It can be seen that the morphology of the filter layers is maintained in the face mask prototypes and that the BC membranes incorporating CeO_2NPs are clearly covering the spaces between the micrometric fibers of PP or cotton. To evaluate the performance of our face mask prototypes, we assessed the filtration efficiency (FE) and breathability, while other important parameters such as fit and seal properties, flammability, and shelf life are beyond the scope of this research report and should be considered in later stages of product development. Likewise, the antioxidant properties of CeO_2NPs might hold greater relevance in alternative medical dressings like bandages or wound dressings, offering skin care protection, such as aiding in the recovery from skin burns, and have not been investigated in the face mask prototypes. The PP@BC@CeO_2NPs layer showed a differential pressure (ΔP) of 8.1 Pa after production, which increased to 25.2 Pa after 24 h of use **(Figure 7c)**. When the additional PP layer was added, the face mask exhibited similar ΔP values after 24 h of use. In the case of the Cotton@BC@CeO_2NPs layer, these values were even lower (ΔP = 1.4 Pa) after production and increased to 4.7 Pa after 24 h of use. With the additional absorbent PP layer, the ΔP values ranged from 4.6 Pa to 11.1 Pa after 24 h of use **(Figure 7f)**. Comparable values were obtained for the PP or cotton layer controls (data not shown), which are typically reported in the literature.[41] These results suggest that the BC@CeO_2NPs fibers do not compromise comfortable breathability due to their high porosity. Furthermore, the FE values for all tested materials were around 70% for 0.3 µm particles, which remained consistent over the following 24 h **(Figure 7c, f)**. This indicates an enhanced FE compared to cotton and PP layers **(Table 1)**,[41-42] probably due to the smaller mesh-size provided by the BC structure.

Additionally, for all evaluated masks, the FE was consistently reported as approximately 100% for larger particles (>3 µm; data not shown).

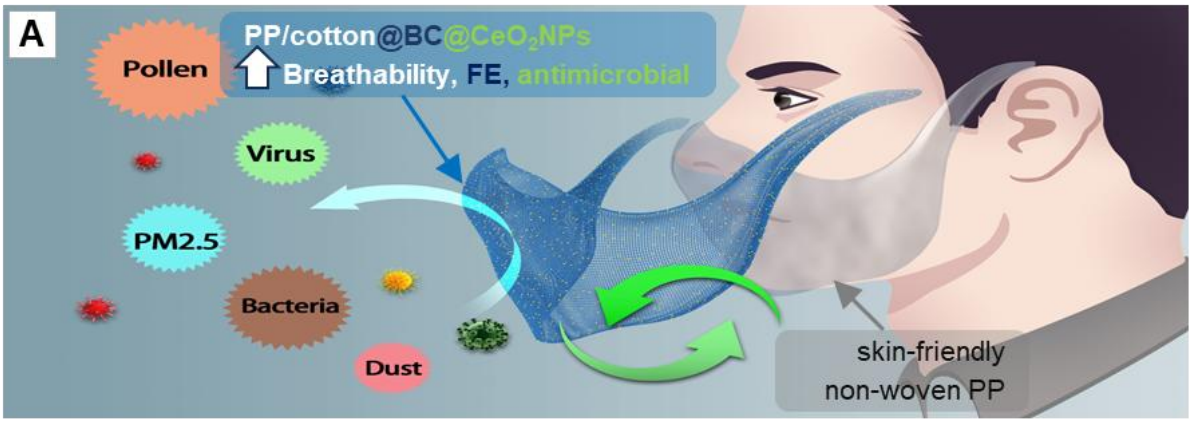
A
Pollen
PP/cotton@BC@CeO2NPs
Breathability, FE, antimicrobial
Virus
PM2.5
Bacteria
Dust
skin-friendly
non-woven PP

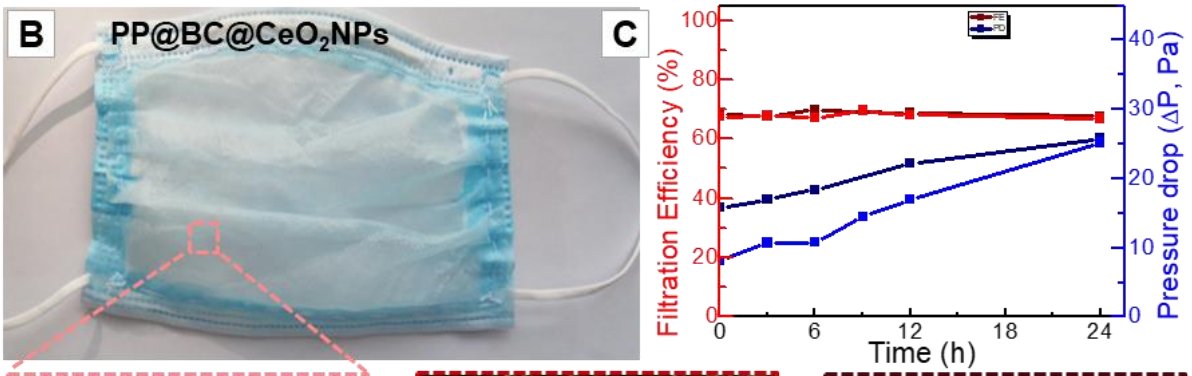
B
PP@BC@CeO2NPs
C
Filtration Efficiency (%)
Pressure drop (ΔP, Pa)
Time (h)

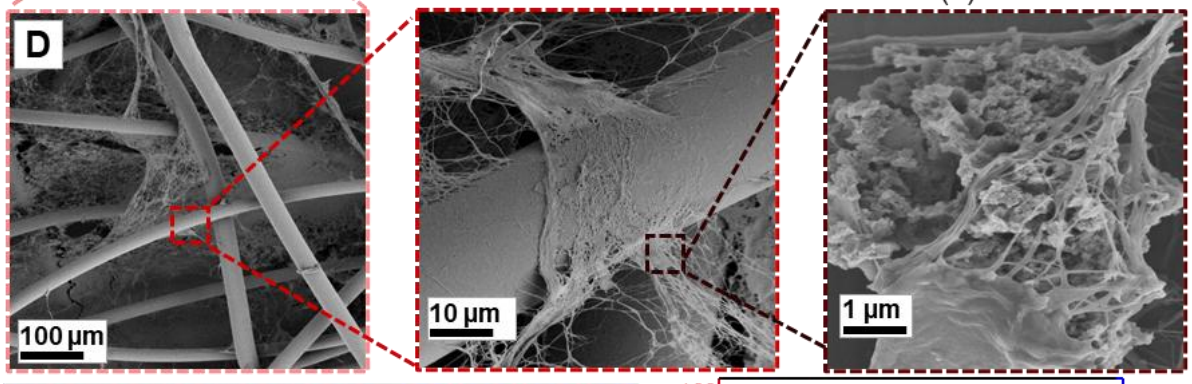
D
100 μm
10 μm
1 μm

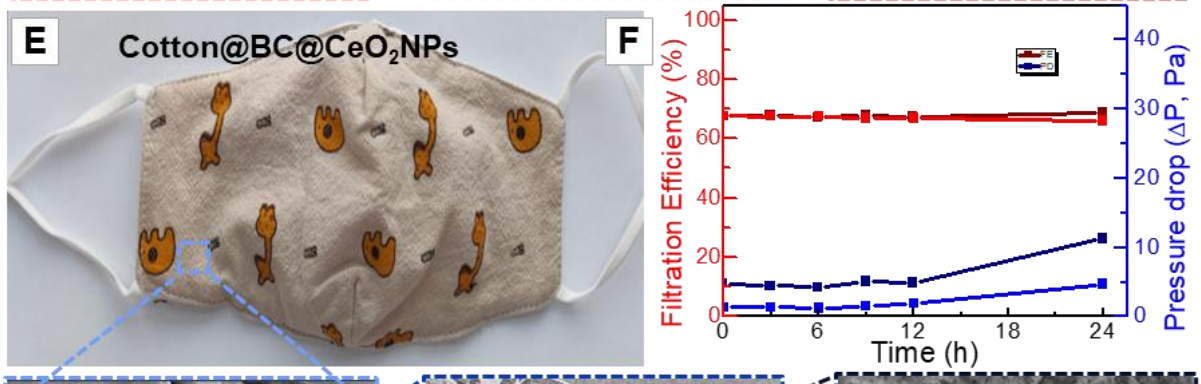
E
Cotton@BC@CeO2NPs
F
Filtration Efficiency (%)
Pressure drop (ΔP, Pa)
Time (h)

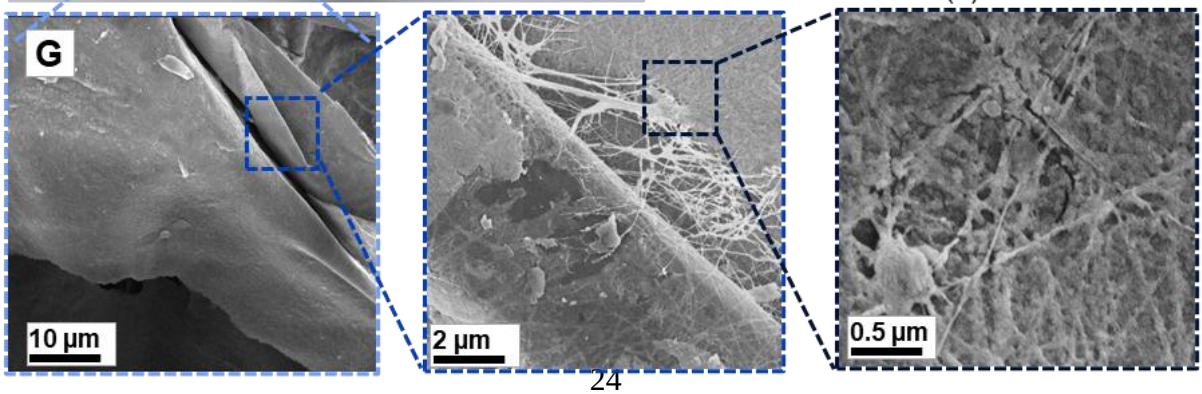
G
10 μm
2 μm
0.5 μm

Figure 7 A. Schematic illustration of the face mask prototypes. **B and E.** Images of the PP/Cotton@BC@CeO_2NPs layer in the face mask prototype. **C and F.** Differential pressure (ΔP) and Filtration Efficiency (FE) for 0.3 μm particles over 24 h of the PP/Cotton@BC@CeO_2NPs layer alone and with the additional skin-friendly PP layer. **D and G.** SEM photographs of the PP/Cotton@BC@CeO_2NPs layer at different magnifications.

In order to function effectively, a face mask should provide an unimpeded breathing experience for the user while concurrently filtering out particulates; however, these characteristics of filtration efficiency and breathability are somewhat diametrically opposed. The distinction between respirator masks and surgical masks offers a paradigmatic illustration of this dichotomy. Respirator masks, such as the KN95 model, are typically comprised of four layers: an external hydrophobic layer designed to filter 0.5 μm particles, an inner absorbent layer commonly made of non-woven materials like PP or analogous synthetic nonbiodegradable polymers, and two central layers – one imbued with activated carbon for chemical filtration, and another of cotton for additional particulate filtering. This design provides a filtration efficacy of at least 95% for particles measuring 0.3 μm, conforming to the face for a secure fit.[37a, 42a, 43] However, the differential pressure (ΔP) can reach as high as 343 Pa, which is the maximum ΔP permissible for an N95 respirator.[44] On the other hand, ASTM F2100, a standard specification for performance materials in medical face masks, posits that for adequate breathability in surgical masks used by healthcare professionals, the maximal allowable ΔP is 58.8 Pa (6 mmH_2O) and the WHO states that Acceptable breathability of a medical mask should be below 49 Pa and below 100 Pa for non-medical masks.[45] Single-use surgical masks, which are the most ubiquitous, afford a looser fit and are primarily engineered to obstruct large respiratory droplets. They deliver a filtration efficiency exceeding 98% for 3.0 μm particles (x), although the efficiency rates for smaller particles fluctuate and are generally lower (between 30–70%).[46] Such masks usually consist of three layers: a filter layer sandwiched between two layers of non-woven fabric. A comprehensive elucidation regarding the maximum ΔP as outlined by various standards, as well as approval requirements and usage, can be gleaned from works such as those by Zhao et al.[41a] and Kwong et al.[46] and summarized in **Table 1**.

Table 1. Comparison of the filter layers and face masks developed in this work with commercially available materials, surgical masks and respirators (data obtained from Zangmeister et al.[42a] and the WHO.[45]

Material	Structure	ΔP (Pa)	FE_{min} (%)	QF (kPa^{-1})
Cotton	plain weave *apparel fabric*	113.7	11.7	1.1
Cotton	plain weave *bandana*	28.4	7.1	2.6
Cotton	poplin weave	32.8	13.3	6.2
Cellulose	Bonded	19	20	5.1
Nylon	plain weave *apparel wool*	55.8	10.9	2.1
Polyester	poplin weave *apparel fabric*	103.9	21.4	2.3
Polypropylene	Spunbound Nonwoven)	1.6	6	16.9
HEPA filter	multi-layer	54.9	94.4	50.2
N95 fabric	multi-layer	228.3	86.0	8.6
N95 mask	multi-layer	79.4	99.9	86.9
Surgical mask	multi-layer	32.8	30.6	11.1
	This work:			
PP@BC@CeO_2 layer	PP: spunbound nonwoven	8.1	67.4	138.6
PP@BC@CeO_2 mask	PP: spunbound nonwoven	15.7	68.4	73.4
Cotton@BC@CeO_2 layer	Cotton: plain weave	4.7	66.1	230.0
Cotton@BC@CeO_2 mask	Cotton: plain weave	11.1	68.3	103.4

Table 1. Filtration efficiency (FE), differential pressure (ΔP) and quality factor (QF) for cloth and synthetic materials used in masks intended for protection from the SARS-CoV-2 virus, and polypropylene-based fiber filter materials including N95 respirators and surgical masks, and comparison with the filter layers and mask developed in this study. Measurements were performed by Zangmeister et al.[42a] and references therein where materials were tested against 50 and 825 nm particle mobility diameters of NaCl aerosol, and the WHO and references therein.[45]

Given that PP is acknowledged for facilitating relatively effective breathability and cotton masks tend to surpass PP masks in this regard, we used and compared both materials in our mask prototypes. The resultant ΔP values for both materials fall comfortably below the specified limits, suggesting good breathability. When these values are coupled with their respective FE values, the quality factor (QF) of our mask prototypes consistently exceeds 100 **(Table 1**), which is markedly higher than what is typically reported in the literature. QF is a relative measure used to assess the overall performance of a filter through the amalgamation of its FE and ΔP at different time points. This measure is typically calculated in line with recommendations from the World Health Organization (WHO),[42a, 45] as follows:

$$QF = \frac{-\ln\left(1 - FEmin/100\right)}{\Delta P}$$

Hence, when observations are made at comparable flow rates, a higher QF signifies superior performance. There has been an exponential surge in research on the QF of fabric and face masks during the COVID-19 pandemic. For instance, a comprehensive study examining the FE and ΔP of 40 different face mask materials aimed at providing protection against the SARS-COV-2 virus found the highest QF to be attributed to the multilayer N95 face mask (approximately 100), with only four materials exhibiting a QF exceeding 10. Interestingly, the study also highlighted that two of the top-performing materials in terms of QF demonstrated a low FE_{min} and ΔP, a characteristic comparable to the conditions exhibited by the PP/Cotton@BC@CeO_2NPs layers and face masks produced in this study. For context, the WHO recommendation according to expert consensus during the COVID-19 pandemic endorsed the use of face masks with a QF > 3.[45]

3. Conclusions

In summary, highly stable BC@CeO_2NPs have been synthesized, the optimal conditions for their preparation have been determined, and the composites showed high antibacterial activity against both gram-positive and gram-negative bacteria and antioxidant properties. Numerous investigations have corroborated either the antibacterial or antioxidant capabilities of CeO_2NPs, yet only a limited number have addressed both attributes concurrently. The mechanism underlying the potential for both pro-oxidant and antioxidant activities has been a subject of discussion. Remarkably, no wound dressings on the market offer combined antibacterial and anti-inflammatory activity. Thus, our research could serve as a proof-of-concept for the future development of cosmetic and medical fabrics, particularly for areas where infections and inflammation frequently coexist, such as in the case of burn skin infections. Moreover, the synthesized BC@CeO_2NPs composite has been used to create new filter layers and antimicrobial face masks that surpass commercially available face masks and mask respirators combining breathability and filtration efficiency values, as a demonstration of how these membranes can be practically used and incorporated into commercially marketed products. In line with the eco-research community's call to adhere to the 3-'Rs': Regulate (life-cycle assessment of manufacture processes, disposal, and sanitization), Reuse, and Replace (transitioning from nonbiodegradable to degradable materials), our BC@CeO_2NPs presents as an eco-friendly, biodegradable compound that could reduce the use of nonbiodegradable materials in face masks and enable mask reusability, as demonstrated in this study.

4. Experimental Section

4.1. Materials: Bacterial strains *Komagataeibacter Xylinus* (BNCC-JCM9730), also known as *Gluconacetobacter xylinus*, *Staphylococcus aureus* (BNCC186335), *Escherichia coli* (BNCC371833) and *Pseudomonas aeruginosa* (BNCC337005) were procured from BeNa Culture Collection, Xinyang City, Henan Province, China. Unless stated otherwise all chemicals and reagents were purchased from Sigma-Aldrich and used as received. For the production of bacterial cellulose (BC), glucose, peptone, yeast extract, agar, Sodium hydroxide (NaOH), Sodium dihydrogen phosphate dodecahydrate ($Na_2HPO_4{\cdot}12H_2O$) and citric acid monohydrate were employed. For the synthesis of the CeO_2NPs, Cerium (III) nitrate hexahydrate ($Ce(NO_3)_3{\cdot}6H_2O$) and Ammonium hydroxide (NH_4OH) were used. For the preparation of the face masks, non-woven polypropylene (PP) and cotton films were supplied by Jiangmen Sure&Me Medical Product Co., Ltd (Jiangmen, China). For cell in-vitro assays, A549 cells were obtained from Shanghai Fuheng Biotechnology Co., Ltd and Dulbecco's Modified Eagle Medium, Foetal Bovine Serum, streptomycin and penicillin were purchased from Sigma-Aldrich. DCFH-DA assay employing 2′,7′-Dichlorofluorescein diacetate cell-permeable redox probe was also used to evaluate the ROS-scavenging properties of the CeO_2NPs synthesized using the optimized microwave-assisted method.

4.2. Production of Bacterial Cellulose (BC): K. xylinus was cultured in a medium consisting of 2% glucose, 0.5% yeast extract, 0.5% yeast peptone, 0.115% anhydrous citric acid, 0.68% $Na_2HPO_4{\cdot}12H_2O$ and 1.5% agar and the preparation of BC films was carried out following our previous work.[2, 18] In a typical procedure, 150 µL of *K. xylinus* was evenly spread on the agar medium and incubated for 48 hours at 28 °C. The *K. xylinus* colony was subsequently transferred to 3 mL of culture medium and incubated for 3 days at 28 °C. After this incubation time, a cellulose film was collected from the air/liquid interface and cleaned. The cleaning process proceeded as follows: initially, BC membranes were transferred to deionized water and boiled for 40 minutes. Subsequently, the membranes were immersed in a solution of 0.1 M NaOH and heated at 90°C for 20 minutes, a cycle repeated four times. Finally,the membranes were neutralized by washing them with deionized water.

4.3. Synthesis of BC@CeO_2NPs composites and CeO_2NPs: BC@CeO_2NPs were synthesized via in-situ chemical deposition of Ce^{3+} precursor in the highly hydroxylated structure of the

BC and the subsequent formation of CeO_2NPs under microwave irradiation. Microwave experiments were carried out using a Monowave 400/500 (Anton Paar). In a typical synthesis, BC membranes harvested after three days of culture using *K. Xylinum* were first immersed for 30 min in microwave-oven flasks containing 9.73 mL of an aqueous solution of $Ce(NO_3)_3 \cdot 6H_2O$ (10 mM) to ensure a homogeneous distribution of the precursor inside the cellulose network. Following this, NH_4OH was added to achieve a final concentration of 27 mM (using 270 µL from a 1M stock solution) as the oxidizing reagent. The mixture underwent heating at a rate of 2 °C/s for 1 minute with stirring at 200 rpm in the microwave reactor, utilizing a maximum power of 350W. Subsequently, the mixture was maintained at 150°C for 3 minutes, maintaining the same stirring rate and microwave power. Temperature and pressure were monitored using a volume-independent infrared sensor. Subsequently, the solution underwent an automatic cooling process to 50 °C using facilitated by compressed nitrogen for approximately 3 minutes. BC@CeO_2NPs films underwent a cleaning procedure in a 10 mL ethanol bath, followed by a 3-minute sonication and subsequent washing with distilled water until neutral pH was achieved. CeO_2NPs that were not incorporated in the BC structure were separated via centrifugation at 12000 rpm for 10 minutes. The prepared BC@CeO_2NPs nanocomposites were stored in deionized water for subsequent characterization. In the experiments detailed in this study, the BC@CeO_2NPs membranes were dried employing two different methods: solvent evaporation at room temperature (BC-RD) and freeze-drying (BC-FD). CeO_2NPs were synthesized under identical conditions in absence of BC.

4.4. Characterization techniques: The synthesized BC, CeO_2NPs, and BC@CeO_2NPs composite were visualized using a high-resolution transmission electron microscopy (HR-TEM, FEI Talos, F200s). 40 µL of the colloidal solutions were drop-casted onto a carbon coated 200 mesh copper grid and allowed to dry at room temperature. Particle size distribution was measured using Image J Analysis software. The morphology of both BC and BC@CeO_2NPs nanocomposites was observed using a JEOL, JSM-5600LV scanning electron microscope with an acceleration voltage of 15 kV. Hydrodynamic diameters were determined with Dynamic Light Scattering (DLS, Nanotrac wave II, Macchique, USA) with a light source wavelength of 532 nm and fixed scattering angle of 173º. Measurements were conducted in 1 cm path cell, and three independent measures were conducted.

The crystallinity and structural phase of the BC, CeO_2NPs, and BC@CeO_2NPs were analyzed using X-ray diffraction analysis (Rigaku SmartLab SE diffractometer, Tokyo, Japan) using Cu Kα (λ =0.15418 nm) in the range of 2θ = 5—90° with an increment of 0.02°. The Fourier-Transform Infrared (FT-IR) spectra were recorded with a Niolet iN10 (Thermo, Guangzhou, China) in transmittance mode. X-ray photoelectron spectroscopy (XPS) was measured with the Thermo Scientific K-Alpha X-ray photoelectron spectrometer (Thermo Fisher Scientific (China) Co., Ltd.) with Al Kα monochromator as an X-ray source.

TGA was carried out using a NETZSCH TG 209 F1 analyzer equipment. The samples underwent heating from 30 to 800 ℃ at a heating rate of 10℃/min under nitrogen atmosphere. Derivative TG curves (DTG) were generated to represent the rate of weight loss as a function of temperature.

Nitrogen sorption isotherms were measured with a ASAP2010 analyzer (Micromeritcs, USA). Before measurements, the samples were dried in a vacuum oven at room temperature for 24 h, and outgassed in the instrument at 60 ℃ for 24 hours. The specific surface areas were calculated by the Brunauer-Emmett-Teller (BET) method in a linear relative pressure range between 0.05 and 0.25. The pore size distributions were derived from the desorption branches of the isotherms by the NLDFT method.

The study of the CeO_2NPs synthesized via the microwave-assisted method, involving variations in temperature, heating rate, MW power and stirring speed was performed with UV-Visible Spectrophotometry (UV-VIS) with a Shimadzu UV-1900 (Japan) spectrophotometer. For analysis, 3 ml of the solution containing the CeO_2NPs was added into a quartz cuvette, and spectra were recorded within the wavelength range of 190-700 nm.

4.5. Fabrication of PP@BC@CeO_2NPs and Cotton @BC@CeO_2NPs filter layers, and face masks: Two different filter layers were fabricated via crosslinking BC@CeO_2NPs with films composed of either spunbound non-woven PP or plain weave cotton. The PP film utilized originated from the inner layer of a face mask that complies with essential performance standards ASTM 2100 (American Society for Testing and Materials), EN 14683:2019+AC:2019 (European standard for face masks) and YY 0469-2011 (from pharmaceutical industry standards of the People's Republic of China) and the plain wave cotton film used had a GSM of 100 g/m^2 and [Warp Count x Weft Count / EPI (ends per inch)

x PPI (picks per inch)] = 40x40/32x30 (moderately dense and tight respectively, for a balance between providing a sufficient barrier while maintaining breathability). For both filter layers, a similar method was followed. Firstly, films of either PP or cotton with 17.5 x 9.5 cm dimensions were cleaned by deionized water to remove the impurities before use. After drying at 60°C for 2 hours, the cleaned films were uniformly distributed. Subsequently, culture media and G. xylinus were evenly spread on the petri dishes and incubated for 16 hours at 28 °C, following the previously described procedure. After this incubation time, filter layers of PP@BC@CeO_2NPs and Cotton @BC@CeO_2NPs crosslinked via strong van der Waals and hydrogen bonding interactions between BC and the PP or cotton fibers[38] were obtained. To perform the in-situ chemical synthesis of CeO_2NPs, these layers were initially immersed for 30 minutes in microwave-oven flasks containing an aqueous solution of $Ce(NO_3)_3 \cdot 6H_2O$ (10 mM). Subsequently, NH_4OH was added, and the optimized MW synthesis of CeO_2NPs on the BC fibrils was carried out following the previously described method. Finally, filter layers samples were purified with 10 mL ethanol bath, sonicated for 3 minutes and washed by distilled water until neutral. Face mask prototypes were fabricated by adding an inner skin-friendly of non-woven PP that met the requirements of the standards specified above.

4.6. Filtration Efficiency and inhalation resistance: To conduct filtration and air permeability tests, samples of PP@BC@CeO_2NPs and cotton@BC@CeO_2NPs filter layers , along with their respective face mask prototypes, were employed. Face masks were assembled in the sequence of the original mask and tested as the filter layers. Filter layers and face masks were tested in Flat Filter mode, and in the case of face masks the assembly was oriented with the inner layer facing the inlet of the filter holder to mimic the passage of exhaled breath through the face mask. The testing conditions were adopted from the ASTM F2299-03 standard test method for determining the initial efficiency of materials used in medical face masks to penetration by particulates according to ASTM F2100:2019.[47] Samples were mounted on a respirator pump and a sampling rate of 15 L/min in both samples and blank lines was set. The flow rate employed is comparable to the typical human breathing rate during light-intensity activities across most of the age groups. Assuming the surface area of 166 cm^2 (17.5x9.5 cm), the corresponding face velocity through the respirator was calculated to be 1.4 cm/s. This face velocity lies in the range of 0.5–25 cm/s, based on the filtration efficiency test standards of ASTM International. A NaCl salt aerosol was used and measured by a Automatic filter material tester (TSI-8127/8130, USA). High resolution channels on the particle counter were

chosen as 0.3 μm, 0.5 μm, 1.0 μm, 5.0 μm, and 10.0 μm and scanned. Polydisperse NaCl aerosol is a common challenge aerosol in filtration studies, and capture efficiencies of the 0.3 μm, 0.5 μm, and 1.0 μm particle sizes are within the most penetrating particle size ranges. The filtration efficiency for each size channel was then calculated using by the following equation:

$$Filtration\ Efficiency, FE\ (\%) = \left[\frac{Cblanck - Cmask}{\text{blank}}\right] * 100\%$$

where C_{blank} is the average salt particle counts at the corresponding size channel without a sample in the filter holder and C_{sample} is the average salt particle counts at the corresponding size channel with the samples in the filter holder.

The test to determine inhalation resistance followed standards EN 14683 and ASTM2100. These standards which set the requirements for the breathability of mask material, measured by the differential pressure across the filter layers and masks. They outline a maximum limit of 35 mm water-column height for this parameter. Each sample was affixed to a funnel (4.5 cm diameter) as is the case of flat samples. A flow rate corresponding to 8 cm/s face velocity (corresponding to 85 liter per minute) was pulled through the material and the pressure drop was measured using a digital manometer.

4.7. Antibacterials tests: The antibacterial activities of CeO_2NPs, BC@CeO_2NPs, and PP@BC@CeO_2NPs and Cotton @BC@CeO_2NPs filter layers against *S. aureus*, *E. coli*, and *P. aeruginosa* were evaluated using OD600 assay, zone of inhibition tests and CFU counting. For the OD600 assay, bacteria were first cultured at 37°C at a concentration of 2×10^8 CFU/mL, and the bacterial suspension were further diluted to 1.5×10^5 CFU/mL (OD_{600}nm around 0.05). Concurrently, circular sections of BC@CeO_2NPs and filter layers (d=1.5 cm) were cleaned in isopropanol, subjected to a 5 min sonication, and subsequently rinsed with distilled water. These circular sections were then immersed in a 200 μL bacterial culture within a 96-well plate and incubated for 1 hour at 100 rpm for bacterial binding assessment.[48] After this treatment, the bacteria-adhered samples were transferred to a new 96-well plate, placed in an incubator at 37°C and the OD_{600}nm values of the culture medium were measured using a microplate reader at different time points to assess the viability of bacteria within each group.[48b] Under control conditions, the three strains reached the stationary phase after approximately 16 hours of incubation. Using this data, the percentage of bacterial growth inhibition attributable to the CeO_2NPs, in comparison to the control samples, was calculated at the 16-h mark using the following formula:

$$Antibacterial\ rate(\%) = \left[1 - \frac{\boldsymbol{S}\mathrm{OD}_{600}(16\ \mathrm{h}) - \boldsymbol{S}\mathrm{OD}_{600}(0\ \mathrm{h})}{\boldsymbol{C}\mathrm{OD}_{600}(16\ \mathrm{h}) - \boldsymbol{C}\mathrm{OD}_{600}(0\ \mathrm{h})}\right] * 100\%$$

where S represents the sample undergoing testing, and C signifies the control, which is the bacteria in their medium. Subsequently, the antibacterial rate in percentage was calculated based on the change in OD_{600} between the control group and the experimental group (samples) at 0-hour and 16-hour time points. Additionally, the number of CFU was correlated with the OD600 measurement (not shown). These tests were replicated three times for each sample.

A second set of experiment was performed by extraction of the surface-adhered bacteria following methods used in previous studies.[49] Briefly, the non-adhered bacteria were washed by gentle rinsing procedure. For the full extraction of bacteria from the samples, the remaining bacteria on the surfaces were extracted using a surfactant/enzyme solution (0.1% sodium dodecyl sulfate (SDS)/PBS solution and 0.5 mL of TrypLE Express enzyme) and sonicated in an ultrasonic bath (50 Hz) for 10 min at 37 °C. Each sample underwent the extraction procedure three times using a fresh extraction solution. The OD_{600} of the extract was measured to calculate the released bacteria, and the number of CFU was then associated with the OD600 measurement. Similar results were obtained using both methods.

The zone of inhibition test was used to qualitatively evaluate the antibacterial activity and the stability of the composites and filter layers. The size of the inhibition zone was measured at least three times for each group, with the bacteria cultured at 37°C to reach 2×10^8 CFU/mL and uniformly plated on agar plates.

4.8. Biocompatibility and ROS-scavenging properties of CeO_2NPs: A549 cells were obtained from American Type Culture Collection (ATCC, Manassas, VA, USA) and seeded in culture plates (5×10^5 cells/well) in Dulbecco's Modified Eagle Medium (DMEM), supplemented with 10% foetal bovine serum (FBS), 50 U/ml penicillin and 50 µg/ml streptomycin, in a humidified atmosphere of 5% CO_2 at 37°C. BC pellicles were added to the wells of 24-well flat bottom culture plates. Subsequently, cells were incubated for 24 hours at 37°C in a 5% CO_2 atmosphere. Similarly, cells were also incubated for 24 hours with CeO_2NPs (10-100 µg/ml). Cell viability was assessed using the MTS (3-(4,5-dimethylthiazol-2-yl)-5-(3-carboxymethoxyphenyl)-2-(4-sulfophenyl)-2H-tetrazolium) technique (CellTiter 96; Promega, Madison, WI, USA) according to the manufacturer's instructions. After being incubated with the CeO_2NPs or BC@CeO_2NPs, cells were washed twice with Hank's Balanced Salt Solution (HBSS). Subsequently, cellTiter reagent was added and cells were

incubated for 4 h at 37°C to allow cells to bioreduce MTS. The absorbance of formazan was measured at 490 nm. To determine the ROS-scavenging ability and 2,7-dichlorofluorescein diacetate (DCFH-DA) probe was used to indicate reactive oxygen species (ROS) generation. Cells (5×10^5 cells/well) were cultured with BC@CeO_2NPs positioned at the well's base or incubated with CeO_2NPs for 24 hours prior exposure to H_2O_2 (400 μM) for an additional 24 hours. Afterward, they were washed 3 times with PBS and were treated with DCFH-DA (10 μM) in dark conditions for 30 minutes at 37°C. Fluorescence images were acquired using an inverted fluorescence microscope (Olympus, China), and quantitative assessments were performed using flow cytometry.

4.9. Statistical analysis: GraphPad Prism 6 (GraphPad Software Inc., San Diego, CA, USA) was employed for the analysis of quantitative data. Statistical assessments were conducted using one-way analysis of variance (ANOVA) accompanied by the Newman-Keuls post hoc test for comparisons among multiple groups. Additionally, the Kruskal-Wallis test, followed by the Dunn post hoc test, was applied when suitable. Results are presented as mean ± standard error of the mean (SEM), with significance determined at a p-value of 0.05 or lower.

Supporting Information

Supporting Information is available from the Wiley Online Library or from the author.

Acknowledgements

The study was financially supported by the National Natural Science Foundation of China (22005221 to M.Z.), the Wuyi University (2018TP010 to E.C., 2018TP011 and 2020FKZX05 to M.Z.), and the Instituto de Salud Carlos III (PI19/00774 and BA22/00017 to G.C., co-funded by the European Regional Development Fund, European Union, "A way to make Europe"). X. Liu, Y. Lin and J. Tang contributed equally to this work.

Conflict of Interest

The authors declare no conflict of interest.

Data Availability Statement

The data that support the findings of this study are available from the corresponding author upon reasonable request.

Received: ((will be filled in by the editorial staff))
Revised: ((will be filled in by the editorial staff))
Published online: ((will be filled in by the editorial staff))

References

[1] a) W. Hu, S. Chen, J. Yang, Z. Li, H. Wang,"Functionalized bacterial cellulose derivatives and nanocomposites", *Carbohydr Polym* **2014**, 101, 1043; b) M. Iguchi, S. Yamanaka, A. Budhiono,"Bacterial cellulose—a masterpiece of nature's arts", *Journal of Materials Science* **2000**, 35, 261; c) D. Klemm, B. Heublein, H.-P. Fink, A. Bohn,"Cellulose: Fascinating Biopolymer and Sustainable Raw Material", *Angewandte Chemie International Edition* **2005**, 44, 3358; d) D. Klemm, F. Kramer, S. Moritz, T. Lindström, M. Ankerfors, D. Gray, A. Dorris,"Nanocelluloses: A New Family of Nature-Based Materials", *Angewandte Chemie International Edition* **2011**, 50, 5438.

[2] M. Zeng, A. Laromaine, A. Roig,"Bacterial cellulose films: influence of bacterial strain and drying route on film properties", *Cellulose* **2014**, 21, 4455.

[3] M. Pang, Y. Huang, F. Meng, Y. Zhuang, H. Liu, M. Du, Q. Ma, Q. Wang, Z. Chen, L. Chen, T. Cai, Y. Cai,"Application of bacterial cellulose in skin and bone tissue engineering", *European Polymer Journal* **2020**, 122, 109365.

[4] S. Sharma, H. Madhyastha, S. S. Kirwale, K. Sakai, Y. T. Katakia, S. Majumder, A. Roy,"Dual antibacterial and anti-inflammatory efficacy of a chitosan-chondroitin sulfate-based in-situ forming wound dressing", *Carbohydrate Polymers* **2022**, 298, 120126.

[5] a) F. Kurtuldu, H. Kaňková, A. M. Beltrán, L. Liverani, D. Galusek, A. R. Boccaccini,"Anti-inflammatory and antibacterial activities of cerium-containing mesoporous bioactive glass nanoparticles for drug-free biomedical applications", *Materials Today Bio* **2021**, 12, 100150; b) Z. Tu, M. Chen, M. Wang, Z. Shao, X. Jiang, K. Wang, Z. Yao, S. Yang, X. Zhang, W. Gao, C. Lin, B. Lei, C. Mao,"Engineering Bioactive M2 Macrophage-Polarized Anti-Inflammatory, Antioxidant, and Antibacterial Scaffolds for Rapid Angiogenesis and Diabetic Wound Repair", *Advanced Functional Materials* **2021**, 31, 2100924; c) Y. Xi, J. Ge, M. Wang, M. Chen, W. Niu, W. Cheng, Y. Xue, C. Lin, B. Lei,"Bioactive Anti-inflammatory, Antibacterial, Antioxidative Silicon-Based Nanofibrous Dressing Enables Cutaneous Tumor Photothermo-Chemo Therapy and Infection-Induced Wound Healing", *ACS Nano* **2020**, 14, 2904; d) C. Kong, S. Chen, W. Ge, Y. Zhao, X. Xu, S. Wang, J. Zhang,"Riclin-Capped Silver Nanoparticles as an Antibacterial and Anti-Inflammatory Wound Dressing", *Int J Nanomedicine* **2022**, 17, 2629.

[6] a) E. Casals, M. Zeng, M. Parra‐Robert, G. Fernández‐Varo, M. Morales‐Ruiz, W. Jiménez, V. Puntes, G. Casals,"Cerium oxide nanoparticles: Advances in biodistribution, toxicity, and preclinical exploration", *Small* **2020**, 16, 1907322; b) S. M. Hirst, A. S. Karakoti, R. D. Tyler, N. Sriranganathan, S. Seal, C. M. Reilly,"Anti‐inflammatory properties of cerium oxide nanoparticles", *Small* **2009**, 5, 2848.

[7] a) P. Bellio, C. Luzi, A. Mancini, S. Cracchiolo, M. Passacantando, L. Di Pietro, M. Perilli, G. Amicosante, S. Santucci, G. Celenza,"Cerium oxide nanoparticles as potential antibiotic adjuvant. Effects of CeO(2) nanoparticles on bacterial outer membrane permeability", *Biochim Biophys Acta Biomembr* **2018**, 1860, 2428; b) M. A. Dar, R. Gul, P. Karuppiah, N. A. Al-Dhabi, A. A. Alfadda,"Antibacterial Activity of Cerium Oxide Nanoparticles against ESKAPE Pathogens", *Crystals* **2022**, 12, 179; c) M. Qi, W. Li, X. Zheng, X. Li, Y. Sun, Y. Wang, C. Li, L. Wang,"Cerium and Its Oxidant-Based Nanomaterials for Antibacterial Applications: A State-of-the-Art Review", *Frontiers in Materials* **2020**, 7; d) M. Zhang, C. Zhang, X. Zhai, F. Luo, Y. Du, C. Yan,"Antibacterial mechanism and activity of cerium oxide nanoparticles", *Science China Materials* **2019**, 62, 1727; e) B. Yuan, Z. Tan, Q. Guo, X. Shen, C. Zhao, J. L. Chen, Y.-K. Peng,"Regulating the H2O2 Activation Pathway on a Well-

Defined CeO2 Nanozyme Allows the Entire Steering of Its Specificity between Associated Enzymatic Reactions", *ACS Nano* **2023**, 17, 17383.

[8] a) C. J. Neal, C. R. Fox, T. S. Sakthivel, U. Kumar, Y. Fu, C. Drake, G. D. Parks, S. Seal,"Metal-Mediated Nanoscale Cerium Oxide Inactivates Human Coronavirus and Rhinovirus by Surface Disruption", *ACS Nano* **2021**, 15, 14544; b) A. Nefedova, K. Rausalu, E. Zusinaite, A. Vanetsev, M. Rosenberg, K. Koppel, S. Lilla, M. Visnapuu, K. Smits, V. Kisand, T. Tätte, A. Ivask,"Antiviral efficacy of cerium oxide nanoparticles", *Scientific Reports* **2022**, 12, 18746; c) M. Zandi, F. Hosseini, A. H. Adli, S. Salmanzadeh, E. Behboudi, P. Halvaei, A. Khosravi, S. Abbasi,"State-of-the-art cerium nanoparticles as promising agents against human viral infections", *Biomedicine & Pharmacotherapy* **2022**, 156, 113868.

[9] a) J.-D. Cafun, K. O. Kvashnina, E. Casals, V. F. Puntes, P. Glatzel,"Absence of Ce3+ Sites in Chemically Active Colloidal Ceria Nanoparticles", *ACS Nano* **2013**, 7, 10726; b) L. M. Ernst, V. Puntes,"How Does Immunomodulatory Nanoceria Work? ROS and Immunometabolism", *Front Immunol* **2022**, 13, 750175; c) F. Esch, S. Fabris, L. Zhou, T. Montini, C. Africh, P. Fornasiero, G. Comelli, R. Rosei,"Electron localization determines defect formation on ceria substrates", *Science* **2005**, 309, 752.

[10] a) I. Gofman, A. Nikolaeva, A. K. Khripunov, A. Yakimansky, E. Ivan'kova, D. P. Romanov, O. Ivanova Polezhaeva, M. Teplonogova, V. Ivanov,"Impact of nano-sized cerium oxide on physico-mechanical characteristics and thermal properties of the bacterial cellulose films", *Nanosystems: Physics, Chemistry, Mathematics* **2018**, 9, 754; b) V. A. Petrova, I. V. Gofman, A. S. Golovkin, A. I. Mishanin, N. V. Dubashynskaya, A. K. Khripunov, E. M. Ivan'kova, E. N. Vlasova, A. L. Nikolaeva, A. E. Baranchikov, Y. A. Skorik, A. V. Yakimansky, V. K. Ivanov,"Bacterial Cellulose Composites with Polysaccharides Filled with Nanosized Cerium Oxide: Characterization and Cytocompatibility Assessment", *Polymers (Basel)* **2022**, 14; c) L. S. R. Rocha, A. Z. Simões, C. Macchi, A. Somoza, G. Giulietti, M. A. Ponce, E. Longo,"Synthesis and defect characterization of hybrid ceria nanostructures as a possible novel therapeutic material towards COVID-19 mitigation", *Scientific Reports* **2022**, 12, 3341; d) J. van Gent González, A. Roig,"Ce 1-x Zr x O 2 nanoparticles in bacterial cellulose, bio-based composites with self-regenerating antioxidant capabilities", *Nanoscale* **2023**, 15; e) N. Melnikova, D. Malygina, V. Korokin, H. Al-Azzawi, D. Zdorova, E. Mokshin, E. Liyaskina, I. Kurgaeva, V. Revin,"Synthesis of Cerium Oxide Nanoparticles in a Bacterial Nanocellulose Matrix and the Study of Their Oxidizing and Reducing Properties", *Molecules* **2023**, 28, 2604.

[11] a) J. Gralton, E. Tovey, M.-L. McLaws, W. D. Rawlinson,"The role of particle size in aerosolised pathogen transmission: A review", *Journal of Infection* **2011**, 62, 1; b) Y. Liu, Z. Ning, Y. Chen, M. Guo, Y. Liu, N. K. Gali, L. Sun, Y. Duan, J. Cai, D. Westerdahl, X. Liu, K. Xu, K.-f. Ho, H. Kan, Q. Fu, K. Lan,"Aerodynamic analysis of SARS-CoV-2 in two Wuhan hospitals", *Nature* **2020**, 582, 557.

[12] Y. Cheng, N. Ma, C. Witt, S. Rapp, P. S. Wild, M. O. Andreae, U. Pöschl, H. Su,"Face masks effectively limit the probability of SARS-CoV-2 transmission", *Science* **2021**, 372, 1439.

[13] a) V. Checchi, M. Montevecchi, L. Valeriani, L. Checchi,"Bioburden Variation of Filtering Face Piece Respirators over Time: A Preliminary Study", *Materials* **2022**, 15, 8790; b) M. Nightingale, M. Mody, A. Rickard, M. Cassone,"Bacterial contamination on used face masks in healthcare personnel", *Antimicrobial Stewardship & Healthcare Epidemiology* **2022**, 2, s86; c) M. Yousefimashouf, R. Yousefimashouf, M. S. Alikhani, H. Hashemi, P. Karami, Z. Rahimi, S. M. Hosseini,"Evaluation of the bacterial contamination of face masks worn by personnel in a center of COVID 19

hospitalized patients: A cross-sectional study", *New Microbes New Infect* **2023**, 52, 101090.

[14] a) V. Bhandari, S. Jose, P. Badanayak, A. Sankaran, V. Anandan,"Antimicrobial Finishing of Metals, Metal Oxides, and Metal Composites on Textiles: A Systematic Review", *Industrial & Engineering Chemistry Research* **2022**, 61, 86; b) S. u. Islam, G. Sun,"Biological Chemicals as Sustainable Materials to Synthesize Metal and Metal Oxide Nanoparticles for Textile Surface Functionalization", *ACS Sustainable Chemistry & Engineering* **2022**, 10, 10084; c) A. K. Yetisen, H. Qu, A. Manbachi, H. Butt, M. R. Dokmeci, J. P. Hinestroza, M. Skorobogatiy, A. Khademhosseini, S. H. Yun,"Nanotechnology in Textiles", *ACS Nano* **2016**, 10, 3042; d) Y. Zhang, X. Xia, K. Ma, G. Xia, M. Wu, Y. H. Cheung, H. Yu, B. Zou, X. Zhang, O. K. Farha, J. H. Xin,"Functional Textiles with Smart Properties: Their Fabrications and Sustainable Applications", *Advanced Functional Materials* **2023**, 33, 2301607.

[15] a) A. M. Eremenko, I. S. Petrik, N. P. Smirnova, A. V. Rudenko, Y. S. Marikvas,"Antibacterial and Antimycotic Activity of Cotton Fabrics, Impregnated with Silver and Binary Silver/Copper Nanoparticles", *Nanoscale Research Letters* **2016**, 11, 28; b) T. Maneerung, S. Tokura, R. Rujiravanit,"Impregnation of silver nanoparticles into bacterial cellulose for antimicrobial wound dressing", *Carbohydrate Polymers* **2008**, 72, 43; c) M. Radetić, D. Marković,"Nano-finishing of cellulose textile materials with copper and copper oxide nanoparticles", *Cellulose* **2019**, 26, 8971; d) K. Geetha, D. Sivasangari, H.-S. Kim, G. Murugadoss, A. Kathalingam,"Electrospun nanofibrous ZnO/PVA/PVP composite films for efficient antimicrobial face masks", *Ceramics International* **2022**, 48, 29197.

[16] a) V. Soni, A. Khosla, P. Singh, V. H. Nguyen, Q. V. Le, R. Selvasembian, C. M. Hussain, S. Thakur, P. Raizada,"Current perspective in metal oxide based photocatalysts for virus disinfection: A review", *J Environ Manage* **2022**, 308, 114617; b) G. A. Sotiriou, S. E. Pratsinis,"Antibacterial Activity of Nanosilver Ions and Particles", *Environmental Science & Technology* **2010**, 44, 5649; c) M. Vincent, R. E. Duval, P. Hartemann, M. Engels-Deutsch,"Contact killing and antimicrobial properties of copper", *J Appl Microbiol* **2018**, 124, 1032.

[17] a) T. M. Benn, P. Westerhoff,"Nanoparticle Silver Released into Water from Commercially Available Sock Fabrics", *Environmental Science & Technology* **2008**, 42, 4133; b) D. M. Mitrano, S. Motellier, S. Clavaguera, B. Nowack,"Review of nanomaterial aging and transformations through the life cycle of nano-enhanced products", *Environment International* **2015**, 77, 132.

[18] M. Zeng, A. Laromaine, W. Feng, P. A. Levkin, A. Roig,"Origami magnetic cellulose: controlled magnetic fraction and patterning of flexible bacterial cellulose", *Journal of Materials Chemistry C* **2014**, 2, 6312.

[19] a) M. Gao, J. Li, Z. Bao, M. Hu, R. Nian, D. Feng, D. An, X. Li, M. Xian, H. Zhang,"A natural in situ fabrication method of functional bacterial cellulose using a microorganism", *Nature Communications* **2019**, 10, 437; b) Q. Zhang, L. Zhang, W. Wu, H. Xiao,"Methods and applications of nanocellulose loaded with inorganic nanomaterials: A review", *Carbohydrate Polymers* **2020**, 229, 115454.

[20] M. Zeng, Y. Shu, M. Parra-Robert, D. Desai, H. Zhou, Q. Li, Z. Rong, D. Karaman, H. Yang, J. Peng, G. Fernandez-Varo, W. Jiménez, G. Casals, V. Puntes, J. M. Rosenholm, E. Casals,"Scalable synthesis of multicomponent multifunctional inorganic core@mesoporous silica shell nanocomposites", *Mater Sci Eng C Mater Biol Appl* **2021**, 128, 112272.

[21] E. G. Heckert, A. S. Karakoti, S. Seal, W. T. Self,"The role of cerium redox state in the SOD mimetic activity of nanoceria", *Biomaterials* **2008**, 29, 2705.

[22] E. Casals, E. Gonzalez, V. F. Puntes,"Reactivity of inorganic nanoparticles in biological environments: insights into nanotoxicity mechanisms", *Journal of Physics D: Applied Physics* **2012**, 45, 443001.

[23] M. Parra-Robert, E. Casals, N. Massana, M. Zeng, M. Perramón, G. Fernández-Varo, M. Morales-Ruiz, V. Puntes, W. Jiménez, G. Casals,"Beyond the Scavenging of Reactive Oxygen Species (ROS): Direct Effect of Cerium Oxide Nanoparticles in Reducing Fatty Acids Content in an In Vitro Model of Hepatocellular Steatosis", *Biomolecules* **2019**, 9.

[24] a) M. L. Foresti, A. Vázquez, B. Boury,"Applications of bacterial cellulose as precursor of carbon and composites with metal oxide, metal sulfide and metal nanoparticles: A review of recent advances", *Carbohydrate Polymers* **2017**, 157, 447; b) J. He, T. Kunitake, A. Nakao,"Facile In Situ Synthesis of Noble Metal Nanoparticles in Porous Cellulose Fibers", *Chemistry of Materials* **2003**, 15, 4401.

[25] A. Karakoti, S. Kuchibhatla, S. B. Krishna Moorthy, S. Seal,"Direct Synthesis of Nanoceria in Aqueous Polyhydroxyl Solutions", *The Journal of Physical Chemistry C* **2007**, 111.

[26] H. Abdullah, M. R. Khan, M. Pudukudy, Z. Yaakob, N. A. Ismail,"CeO2-TiO2 as a visible light active catalyst for the photoreduction of CO2 to methanol", *Journal of Rare Earths* **2015**, 33, 1155.

[27] Z. Fan, F. Meng, J. Gong, H. Li, Y. Hu, D. Liu,"Enhanced photocatalytic activity of hierarchical flower-like CeO2/TiO2 heterostructures", *Materials Letters* **2016**, 175, 36.

[28] J. George, K. V. Ramana, S. N. Sabapathy, J. H. Jagannath, A. S. Bawa,"Characterization of chemically treated bacterial (Acetobacter xylinum) biopolymer: some thermo-mechanical properties", *Int J Biol Macromol* **2005**, 37, 189.

[29] M. Carltonbird, S. Eaimsumang, S. Pongstabodee, S. Boonyuen, S. Smith, A. Luengnaruemitchai,"Effect of the exposed ceria morphology on the catalytic activity of gold/ceria catalysts for the preferential oxidation of carbon monoxide", *Chemical Engineering Journal* **2018**, 344.

[30] K. M. Kumar, M. Mahendhiran, M. C. Diaz, N. Hernandez-Como, A. Hernandez-Eligio, G. Torres-Torres, S. Godavarthi, L. M. Gomez,"Green synthesis of Ce3+ rich CeO2 nanoparticles and its antimicrobial studies", *Materials Letters* **2018**, 214, 15.

[31] a) C. Xu, X. Qu,"Cerium oxide nanoparticle: a remarkably versatile rare earth nanomaterial for biological applications", *NPG Asia Materials* **2014**, 6, e90; b) M. Zeng, X. Zhang, J. Tang, X. Liu, Y. Lin, D. Guo, Y. Zhang, S. Ju, G. Fernández-Varo, Y.-C. Wang, X. Zhou, G. Casals, E. Casals,"Conservation of the enzyme-like activity and biocompatibility of CeO2 nanozymes in simulated body fluids", *Nanoscale* **2023**, 15, 14365.

[32] K. S. Babu, M. Anandkumar, T. Y. Tsai, T. H. Kao, B. S. Inbaraj, B. H. Chen,"Cytotoxicity and antibacterial activity of gold-supported cerium oxide nanoparticles", *Int J Nanomedicine* **2014**, 9, 5515.

[33] E. Heckert, A. Karakoti, S. Seal, W. Self,"The role of cerium redox state in the SOD mimetic activity of nanoceria", *Biomaterials* **2008**, 29, 2705.

[34] R. W. Tarnuzzer, J. Colon, S. Patil, S. Seal,"Vacancy engineered ceria nanostructures for protection from radiation-induced cellular damage", *Nano Letters* **2005**, 5, 2573.

[35] A. Karakoti, S. Singh, J. M. Dowding, S. Seal, W. T. Self,"Redox-active radical scavenging nanomaterials", *Chemical Society Reviews* **2010**, 39, 4422.

[36] a) A. Arumugam, C. Karthikeyan, A. S. Haja Hameed, K. Gopinath, S. Gowri, V. Karthika,"Synthesis of cerium oxide nanoparticles using Gloriosa superba L. leaf extract and their structural, optical and antibacterial properties", *Materials Science and Engineering: C* **2015**, 49, 408; b) D. A. Pelletier, A. K. Suresh, G. A. Holton, C. K.

McKeown, W. Wang, B. Gu, N. P. Mortensen, D. P. Allison, D. C. Joy, M. R. Allison, S. D. Brown, T. J. Phelps, M. J. Doktycz,"Effects of engineered cerium oxide nanoparticles on bacterial growth and viability", *Appl Environ Microbiol* **2010**, 76, 7981; c) A. Thill, O. Zeyons, O. Spalla, F. Chauvat, J. Rose, M. Auffan, A. M. Flank,"Cytotoxicity of CeO2 Nanoparticles for Escherichia coli. Physico-Chemical Insight of the Cytotoxicity Mechanism", *Environmental Science & Technology* **2006**, 40, 6151.

[37] a) V. Palmieri, F. De Maio, M. De Spirito, M. Papi,"Face masks and nanotechnology: Keep the blue side up", *Nano Today* **2021**, 37, 101077; b) F. Seidi, C. Deng, Y. Zhong, Y. Liu, Y. Huang, C. Li, H. Xiao,"Functionalized Masks: Powerful Materials against COVID-19 and Future Pandemics", *Small* **2021**, 17, e2102453.

[38] a) M. Kılınç, E. Ay, D. Kut,"Thermal, Chemical and Mechanical Properties of Regenerated Bacterial Cellulose Coated Cotton Fabric", *Journal of Natural Fibers* **2021**, 19, 1; b) A. Meftahi, R. Khajavi, A. Rashidi, M. Sattari, M. Yazdanshenas, M. Torabi,"The effects of cotton gauze coating with microbial cellulose", *Cellulose* **2010**, 17, 199; c) J. Zhao, B. Deng, M. Lv, J. Li, Y. Zhang, H. Jiang, C. Peng, J. Li, J. Shi, Q. Huang, C. Fan,"Graphene oxide-based antibacterial cotton fabrics", *Adv Healthc Mater* **2013**, 2, 1259.

[39] K. Ardon-Dryer, J. Warzywoda, R. Tekin, J. Biros, S. Almodovar, B. L. Weeks, L. J. Hope-Weeks, A. Sacco, Jr.,"Mask Material Filtration Efficiency and Mask Fitting at the Crossroads: Implications during Pandemic Times", *Aerosol and Air Quality Research* **2021**, 21, 200571.

[40] T. Ristic, L. Zemljič, M. Novak Babič, M. Kralj Kuncic, S. Sonjak, N. Gunde-cimerman, S. Strnad, **2011**, p. 37.

[41] a) M. Zhao, L. Liao, W. Xiao, X. Yu, H. Wang, Q. Wang, Y. L. Lin, F. S. Kilinc-Balci, A. Price, L. Chu, M. C. Chu, S. Chu, Y. Cui,"Household Materials Selection for Homemade Cloth Face Coverings and Their Filtration Efficiency Enhancement with Triboelectric Charging", *Nano Letters* **2020**, 20, 5544; b) K. Goodge, J. L. Du Puis, M. Maher, M. W. Frey, F. Baytar, H. Park,"Cloth face mask fit and function for children part two: Material Selection", *Fashion and Textiles* **2022**, 9, 41.

[42] a) C. D. Zangmeister, J. G. Radney, E. P. Vicenzi, J. L. Weaver,"Filtration Efficiencies of Nanoscale Aerosol by Cloth Mask Materials Used to Slow the Spread of SARS-CoV-2", *ACS Nano* **2020**, 14, 9188; b) S. Sankhyan, K. N. Heinselman, P. N. Ciesielski, T. Barnes, M. E. Himmel, H. Teed, S. Patel, M. E. Vance,"Filtration Performance of Layering Masks and Face Coverings and the Reusability of Cotton Masks after Repeated Washing and Drying", *Aerosol and Air Quality Research* **2021**, 21, 210117.

[43] A. Tcharkhtchi, N. Abbasnezhad, M. Zarbini Seydani, N. Zirak, S. Farzaneh, M. Shirinbayan,"An overview of filtration efficiency through the masks: Mechanisms of the aerosols penetration", *Bioact Mater* **2021**, 6, 106.

[44] a) Determination of Particulate Filter Efficiency Level for N95 Series Filters Against Solid Particulates for Non-Powdered, Air-Purifying Respirators Standard Testing Procedure (STP); TEB-APR-STP-0059; National Institute for Occupational Safety and Health: Pittsburgh, PA, 2019; pp 1−9. https://wwwn.cdc.gov/PPEInfo/Standards/Info/TEBAPRSTP0059, accessed: 2023-09-24; b) Determination of Inhalation Resistance TEB-APR-STP-0007; National Institute for Occupational Safety and Health: Pittsburgh, PA, 2019; pp 1−7. https://wwwn.cdc.gov/PPEInfo/Standards/Info/TEBAPRSTP0007, accessed: 2023-09-24.

[45] Health Emergencies Preparedness and Response Team. Advice on the Use of Masks in the Context of COVID-19: Interim Guidance, 5 June 2020; WHO, 2020.

https://reliefweb.int/attachments/5666ae00-fb5d-3f5b-8cea-4ff4dda46d82/Advice%20on%20the%20use%20of%20masks%20in%20the%20context%20of%20COVID-19.pdf, accessed: 2023-09-24.

[46] L. H. Kwong, R. Wilson, S. Kumar, Y. S. Crider, Y. Reyes Sanchez, D. Rempel, A. Pillarisetti,"Review of the Breathability and Filtration Efficiency of Common Household Materials for Face Masks", *ACS Nano* **2021**, 15, 5904.

[47] ASTM F2100 Standard Specification for Performance of Materials Used in Medical Face Masks https://www.astm.org/f2100-23.htmlz, accessed: 2023-09-24.

[48] a) H. Haase, L. Jordan, L. Keitel, C. Keil, B. Mahltig,"Comparison of methods for determining the effectiveness of antibacterial functionalized textiles", *PLOS ONE* **2017**, 12, e0188304; b) Y. Wang, Q. Yuan, M. Li, Y. Tang,"Cationic Conjugated Microporous Polymers Coating for Dual-Modal Antimicrobial Inactivation with Self-Sterilization and Reusability Functions", *Advanced Functional Materials* **2023**, 33, 2213440.

[49] S. K. Bopp, T. Lettieri,"Comparison of four different colorimetric and fluorometric cytotoxicity assays in a zebrafish liver cell line", *BMC Pharmacol* **2008**, 8, 8.

The table of contents entry.

Versatile Antibacterial and Antioxidant Bacterial Cellulose@Nanoceria Biotextile and its Application in Antimicrobial Face Masks with Recyclability and Reusability Functions

J. Tang, Y. Zhang, X. Liu, Y. Lin, L. Liang, X. Li, G. Casals, X. Zhou*, E. Casals*, M. Zeng**

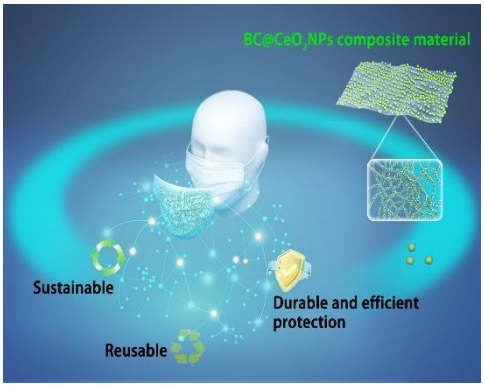

A comprehensive exploration of the optimal parameters for producing innovative Bacterial Cellulose membranes covalently-linked with controllable quantities of small-sized CeO_2NPs (BC@CeO_2NPs) is performed. This composite biotextile has been used to develop antimicrobial face masks and has the potential to pave the way for the development of medical and cosmetic dressings that offer a combination of antibiotic and anti-inflammatory properties.